4

Parameter Estimation: Applications

Errors using inadequate data are much less than those using no data at all. Babbage, Charles

THE previous chapters laid down the foundation for the application of parameter estimation methods to dynamical systems. In this chapter several example applications are presented in which the methods of the first two chapters can be used to advantage with the class of dynamical systems discussed in the previous chapter. The problems and solutions are idealizations of "real-world" applications that are well-documented in the literature cited. First, the position of a vehicle is determined using Global Positioning System (GPS) signals transmitted from orbiting spacecraft. Then, spacecraft attitude determination is introduced using photographs of stars made from one or more spacecraft-fixed cameras. Next, spacecraft orbit determination from ground radar observations using a Gaussian Least Squares Differential Correction (GLSDC) is presented. Then, parameter estimation of an aircraft using various sensors is introduced. Finally, flexible structure modal realization using the Eigensystem Realization Algorithm (ERA) is studied. This chapter shows only the fundamental concepts of these applications; the emphasis here is upon the utility of the estimation methodology. However, the examples are presented in sufficient detail to serve as a foundation for each of the subject areas shown. The interested reader is encouraged to pursue these subjects in more depth by studying the many references cited in this chapter.

4.1 Global Positioning System Navigation

The Global Positioning System (GPS) constellation was originally developed to permit a wide variety of user vehicles an accurate means of determining position for autonomous navigation. The constellation includes 24 space vehicles (SVs) in known semi-synchronous (12-hour) orbits, providing a minimum of six SVs in view for ground-based navigation. The underlying principle involves geometric triangulation with the GPS SVs as known reference points to determine the user's position to a high degree of accuracy. The GPS was originally intended for ground-based and aviation applications, and is gaining much attention in the commercial commu-

nity (e.g., automobile navigation, aircraft landing, etc.). However, in recent years there has been a growing interest in other applications, such as spacecraft navigation, attitude determination, and even as a vibration sensor. Since the GPS SVs are in approximately 20,000 km circular orbits, the position of any potential user below the constellation may be easily determined.

A minimum of four SVs are required so that, in addition to the three-dimensional position of the user, the time of the solution can be determined and in turn employed to correct the user's clock. Since its original inception, there have been many innovative improvements to the accuracy of the GPS determined position. These include using local area as well as wide area differential GPS and carrier-phase differential GPS. In particular, carrier-phase differential GPS measures the phase of the GPS carrier relative to the phase at a reference site, which dramatically improves the position accuracy. These innovative techniques allow for more accurate GPS determined positions.

The fundamental signal in GPS is the pseudo-random code (PRC) which is a complicated binary sequence of pulses. Each SV has its own complex PRC, which guarantees that the receiver won't be confused with another SV's signal. The GPS satellites transmit signals on two carrier frequencies: L1 at 1575.42 MHz and L2 at 1227.60 MHz. The modulated PRC at the L1 carrier is called the Coarse Acquisition (C/A) code, which repeats every 1023 bits and modulates at a 1MHz rate. The C/A code is the basis for civilian GPS use. Another PRC is called the Precise (P) code, which repeats on a seven-day cycle and modulates both the L1 and L2 carriers at a 10 MHz rate. This code is intended for military users and can be encrypted. Position location is made possible by comparing how late in time the SV's PRC appears to the receiver's code. Multiplying the travel time by the speed of light, one obtains the distance to the SV. This requires very accurate timing in the receiver, which is provided by using a fourth SV to correct a "clock bias" in the internal clock receiver.

There are many error sources that affect the GPS accuracy using the PRC. First, the GPS signal slows down slightly as it passes through the charged particles of the ionosphere and then through the water vapor in the troposphere. Second, the signal may bounce off various local obstructions before it arrives at the receiver (known as *multipath* errors). Third, SV ephemeris (i.e., known satellite position) errors can contribute to GPS location inaccuracy. Finally, the basic geometry on the available SVs can magnify errors, which is known as the Geometric Dilution of Precision (GDOP). A poor GDOP usually means that the SV sightlines to the receiver are close to being collinear, resulting in degraded accuracy. Many of the aforementioned errors can be minimized or even eliminated by using differential GPS.

Differential GPS (DGPS) involves the cooperation of two receivers, one that is stationary and another that is moving to make the position measurements. The basic principle incorporates the notion that two receivers will have virtually the same errors if they are fairly close to one another (within a few hundred kilometers). The stationary receiver uses its known (calibrated) position to calculate a timing difference (error correction) from the GPS determined position. This receiver then transmits this error information to the moving receiver, so that an updated position correction can be made. DGPS minimizes ionospheric and tropospheric errors, while virtually

Table 4.1: Levels of GPS Accuracy

Technique	Method	Accuracy
PRC	measure signal time-of-flight from each SV	10 to 100 m (absolute)
DGPS	difference of the time-of-flight between two receivers	1 to 5 m (relative)
CDGPS	reconstruct carrier and measure relative phase difference between two antennae	≤ 5 cm for kinematic (relative) ≤ 1 cm for static (relative)

eliminating SV clock errors, and ephemeris errors. Accuracies of 1 to 5 meters can be obtained using DGPS.

Carrier-Phase Differential GPS (CDGPS) can be used to further enhance the position determination performance. The PRC has a bit rate of about 1 MHz but its carrier frequency has a cycle rate of over 1 GHz. At the speed of light the 1.57 GHz GPS carrier signal has a wavelength of about 20 cm. Therefore, by obtaining 1% perfect phase, as is done in PRC receivers, accuracies in the mm region are possible. CDGPS measures the phase of the GPS carrier relative to the carrier phase at a reference site. If the GPS antennae are fixed, then the system is called static, and mm accuracies are typically possible since long averaging times can be used to filter any noise present. If the antennae are moving, then the system is kinematic, and cm accuracies are possible since shorter time constants are used in the averaging. Since phase differences are used, the correct number of integer wavelengths between a given pair of antennae must first be found (known as "integer ambiguity resolution"). CDGPS can also be used for attitude determination of static or moving vehicles. A chart summarizing the various levels of GPS accuracy is shown in Table 4.1.

The equations needed to be solved to determine a user's position (x, y, z) and clock bias τ (in equivalent distance) from GPS pseudorange measurements are given by

$$\boxed{\tilde{\rho}_i = [(e_{1i} - x)^2 + (e_{2i} - y)^2 + (e_{3i} - z)^2]^{1/2} + \tau + v_i, \ i = 1, 2, \ldots, n} \qquad (4.1)$$

where (e_{1i}, e_{2i}, e_{3i}) are the known i^{th} GPS satellite coordinates, n is the total number of observed GPS satellites, and v_i are the measurement errors which are assumed to be the same for each satellite and represented by a zero-mean Gaussian noise process with variance σ^2. Because the number of unknowns is four with $\mathbf{x} = \begin{bmatrix} x & y & z & \tau \end{bmatrix}^T$, at least four non-parallel SVs are required to solve eqn. (4.1).

Since eqn. (4.1) represents a nonlinear function of the unknowns, then nonlinear least squares must be utilized. The estimated pseudorange $\hat{\rho}$ is determined by using the current position estimates $(\hat{x}, \hat{y}, \hat{z})$ and clock bias $\hat{\tau}$ estimate, given by

$$\hat{\rho}_i = [(e_{1i} - \hat{x})^2 + (e_{2i} - \hat{y})^2 + (e_{3i} - \hat{z})^2]^{1/2} + \hat{\tau} \tag{4.2}$$

The i^{th} row of H is formed by taking the partials of eqn. (4.1) with respect to the unknown variables, so that

$$H = \begin{bmatrix} \frac{\partial \hat{\rho}_1}{\partial \hat{x}} & \frac{\partial \hat{\rho}_1}{\partial \hat{y}} & \frac{\partial \hat{\rho}_1}{\partial \hat{z}} & 1 \\ \frac{\partial \hat{\rho}_2}{\partial \hat{x}} & \frac{\partial \hat{\rho}_2}{\partial \hat{y}} & \frac{\partial \hat{\rho}_2}{\partial \hat{z}} & 1 \\ \vdots & \vdots & \vdots & \vdots \\ \frac{\partial \hat{\rho}_n}{\partial \hat{x}} & \frac{\partial \hat{\rho}_n}{\partial \hat{y}} & \frac{\partial \hat{\rho}_n}{\partial \hat{z}} & 1 \end{bmatrix} \tag{4.3}$$

The partials are straightforward, with

$$\frac{\partial \hat{\rho}_i}{\partial \hat{x}} = -\frac{(e_{1i} - \hat{x})}{[(e_{1i} - \hat{x})^2 + (e_{2i} - \hat{y})^2 + (e_{3i} - \hat{z})^2]^{1/2}} \tag{4.4a}$$

$$\frac{\partial \hat{\rho}_i}{\partial \hat{y}} = -\frac{(e_{2i} - \hat{y})}{[(e_{1i} - \hat{x})^2 + (e_{2i} - \hat{y})^2 + (e_{3i} - \hat{z})^2]^{1/2}} \tag{4.4b}$$

$$\frac{\partial \hat{\rho}_i}{\partial \hat{z}} = -\frac{(e_{3i} - \hat{z})}{[(e_{1i} - \hat{x})^2 + (e_{2i} - \hat{y})^2 + (e_{3i} - \hat{z})^2]^{1/2}} \tag{4.4c}$$

Equations (4.2) to (4.4) are used in nonlinear least squares of §1.4 to determine the position of the user and clock bias. The covariance of the estimate errors is simply given by

$$\boxed{P = \sigma^2 (H^T H)^{-1}} \tag{4.5}$$

The matrix $A \equiv (H^T H)^{-1}$ can be used to define several DOP quantities,[1] including; geometrical DOP (GDOP), position DOP (PDOP), horizontal DOP (HDOP), vertical DOP (VDOP), and time DOP (TDOP), each given by

$$\text{GDOP} \equiv \sqrt{A_{11} + A_{22} + A_{33} + A_{44}} \tag{4.6a}$$

$$\text{PDOP} \equiv \sqrt{A_{11} + A_{22} + A_{33}} \tag{4.6b}$$

$$\text{HDOP} \equiv \sqrt{A_{11} + A_{22}} \tag{4.6c}$$

$$\text{VDOP} \equiv \sqrt{A_{33}} \tag{4.6d}$$

$$\text{TDOP} \equiv \sqrt{A_{44}} \tag{4.6e}$$

The quantity GDOP is most widely used since it gives an indication of the basic geometry of the available SVs and the effect of clock bias errors. The best possible value for GDOP with four available satellites is obtained when one satellite is

directly overhead and the remaining are spaced equally at the minimum elevation angles around the horizon.[2] We note in passing that other observability measures are possible. For example, we could use the condition number of A, which is the ratio of the largest singular value to the least singular value of A. The smallest condition number is unity (for perfectly conditioned orthogonal matrices) and the largest is infinity (for singular matrices).

Example 4.1: In this example nonlinear least squares is employed to determine the position of a vehicle on the Earth from GPS pseudorange measurements. The vehicle is assumed to have coordinates of 38°N and 77°W (i.e., in Washington, DC). Converting this latitude and longitude into the Earth-Centered-Earth-Fixed (ECEF) frame[3] (see §7.1.1 for more details), and assuming a clock bias of 85,000 m gives the true vector as

$$\mathbf{x} = \begin{bmatrix} 1,132,049 & -4,903,445 & 3,905,453 & 85,000 \end{bmatrix}^T \text{ m}$$

At epoch the following GPS satellites and position vector in ECEF coordinates are available:

SV	e_1 (meters)	e_2 (meters)	e_3 (meters)
5	15,764,733	−1,592,675	21,244,655
13	6,057,534	−17,186,958	19,396,689
18	4,436,748	−25,771,174	1,546,041
22	−9,701,586	−19,687,467	15,359,118
26	23,617,496	−11,899,369	1,492,340
27	14,540,070	−12,201,965	18,352,632

The SV label is the specific GPS satellite number. Simulated pseudorange measurements are computed using eqn. (4.1) with a standard deviation on the measurement error of 5 meters. The nonlinear least squares routine is then initiated with starting conditions of 0 for all elements of $\hat{\mathbf{x}}$. The algorithm converges in five iterations. Results of the iterations are given below.

Iteration	$\hat{x}$ (meters)	$\hat{y}$ (meters)	$\hat{z}$ (meters)	Clock (meters)
0	0	0	0	0
1	1,417,486	−5,955,318	4,745,294	1,502,703
2	1,146,483	−4,944,222	3,938,182	143,265
3	1,132,071	−4,903,503	3,905,503	85,085
4	1,132,042	−4,903,436	3,905,448	85,000
5	1,132,042	−4,903,436	3,905,448	85,000

The 3σ estimate-error bounds are given by

$$3\boldsymbol{\sigma} = \begin{bmatrix} 21.3 & 32.1 & 21.1 & 28.3 \end{bmatrix}^T \text{ m}$$

The estimate errors are clearly within the 3σ bounds. In general, the accuracy can be improved if more satellites are used in the solution.

4.2 Attitude Determination

Attitude determination refers to the identification of a proper orthogonal rotation matrix so that the measured observations in the sensor frame equal the reference frame observations mapped by that matrix into the sensor frame. If all the measured and reference vectors are error free, then the rotation (attitude) matrix is the same for all sets of observations. However, if measurement errors exist, then a least-squares type approach must be used to determine the attitude. Several attitude sensors exist, including: three-axis magnetometers, sun sensors, Earth-horizon sensors, global positioning system (GPS) sensors, and star cameras. In this next section we focus on vector measurement models for star cameras (which can also be applied to sun sensors, three-axis magnetometers and Earth-horizon sensors as well).

4.2.1 Vector Measurement Models

With reference to Figure 4.1, we consider the problem of determining the angular orientation of a space vehicle from photographs of the stars made from one or more spacecraft-fixed cameras. The stars are assumed to be inertially fixed neglecting the effects of proper motion and velocity abberation. The brightest 250,000 stars' spherical coordinate angles (α is the right ascension and δ is the declination, see Figure 4.2) are available in a computer accessible catalog.[4] Referring to Figures 4.2, 4.3, and 3.5, given the camera orientation angles (ϕ, θ, ψ), it is established in Ref. [5] that the photograph image plane coordinates of the j^{th} star are determined by the stellar *collinearity equations*:

$$x_j = -f\left(\frac{A_{11}r_{x_j} + A_{12}r_{y_j} + A_{13}r_{z_j}}{A_{31}r_{x_j} + A_{32}r_{y_j} + A_{33}r_{z_j}}\right) \tag{4.7a}$$

$$y_j = -f\left(\frac{A_{21}r_{x_j} + A_{22}r_{y_j} + A_{23}r_{z_j}}{A_{31}r_{x_j} + A_{32}r_{y_j} + A_{33}r_{z_j}}\right) \tag{4.7b}$$

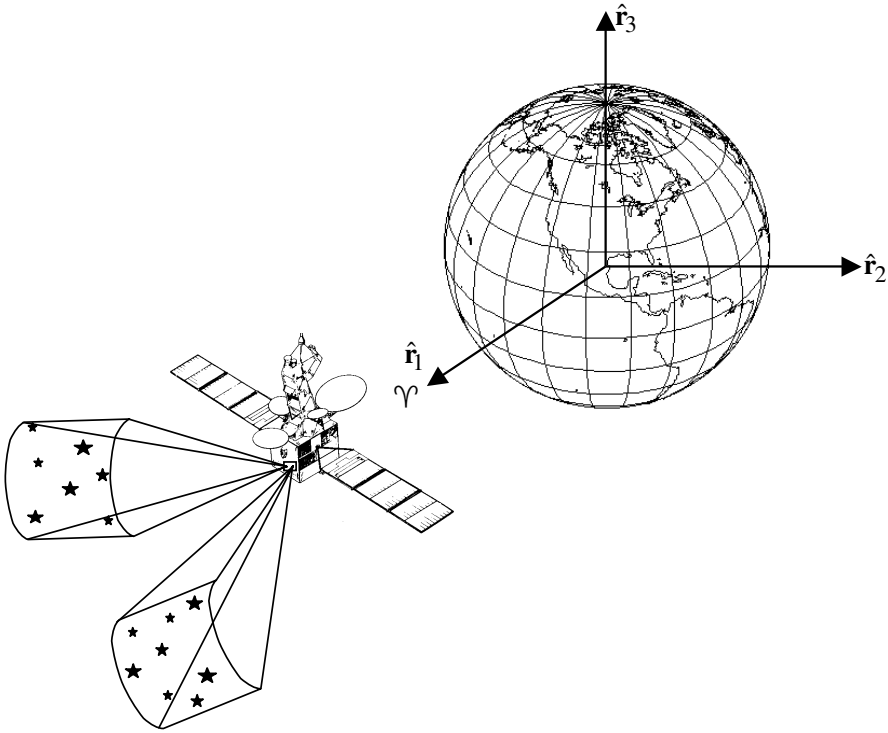

Figure 4.1: Spacecraft Attitude Estimation from Star Photography

where A_{ij} are elements of the attitude matrix A, and the inertial components of the vector toward the j^{th} star are

$$\begin{aligned} r_{x_j} &= \cos\delta_j \cos\alpha_j \\ r_{y_j} &= \cos\delta_j \sin\alpha_j \\ r_{z_j} &= \sin\delta_j \end{aligned} \tag{4.8}$$

and the camera focal length f is known from *a priori* calibration. Note that in this section the vector $\mathbf{r}$ denotes the reference frame, which may be any general frame (e.g., the ECEF frame). When using stars for attitude determination the reference frame coincides with the inertial frame shown in Figures 3.8 and 3.9.

Unfortunately, (ϕ, θ, ψ) are usually not known or poorly known, but if the measured stars can be identified* as specific cataloged stars, then the attitude matrix (and associated camera orientation angles) can be determined from the measured stars in image coordinates and identified stars in inertial coordinates. Clearly, this

*See Ref. [6] for a pattern recognition technique that can be employed to automate the association of the measured images with the cataloged stars.

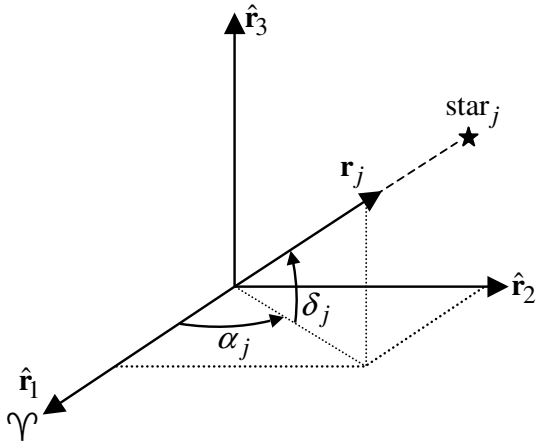

Figure 4.2: Spherical Coordinates Orienting the Line of Sight Vector to a Star

can be accomplished using the nonlinear least squares approach of §1.4. However, through judicious change of variables, a linear form of eqns. (4.7) can be constructed. Choosing the z-axis of the image coordinate system, consistent with Figure 4.3, to be directed outward along the boresight, then the star observation can be reconstructed in unit vector form as

$$\boxed{\mathbf{b}_j = A\mathbf{r}_j, \quad j = 1, 2, \ldots, N} \tag{4.9}$$

where

$$\mathbf{b}_j \equiv \frac{1}{\sqrt{f^2 + x_j^2 + y_j^2}} \begin{bmatrix} -x_j \\ -y_j \\ f \end{bmatrix} \tag{4.10a}$$

$$\mathbf{r}_j \equiv \begin{bmatrix} r_{x_j} & r_{y_j} & r_{z_j} \end{bmatrix}^T \tag{4.10b}$$

and N is the total number of star observations. The components of $\mathbf{b}$ can be written using eqn. (3.142a). When measurement noise is present, Shuster[7] has shown that nearly all the probability of the errors is concentrated on a very small area about the direction of $A\mathbf{r}_j$, so the sphere containing that point can be approximated by a tangent plane, characterized by

$$\tilde{\mathbf{b}}_j = A\mathbf{r}_j + \boldsymbol{\upsilon}_j, \quad \boldsymbol{\upsilon}_j^T A\mathbf{r}_j = 0 \tag{4.11}$$

where $\tilde{\mathbf{b}}_j$ denotes the j^{th} star measurement, and the sensor error $\boldsymbol{\upsilon}_j$ is approximately Gaussian which satisfies

$$E\left\{\boldsymbol{\upsilon}_j\right\} = \mathbf{0} \tag{4.12a}$$

$$E\left\{\boldsymbol{\upsilon}_j \boldsymbol{\upsilon}_j^T\right\} = \sigma_j^2 \left[I_{3\times 3} - (A\mathbf{r}_j)(A\mathbf{r}_j)^T\right] \tag{4.12b}$$

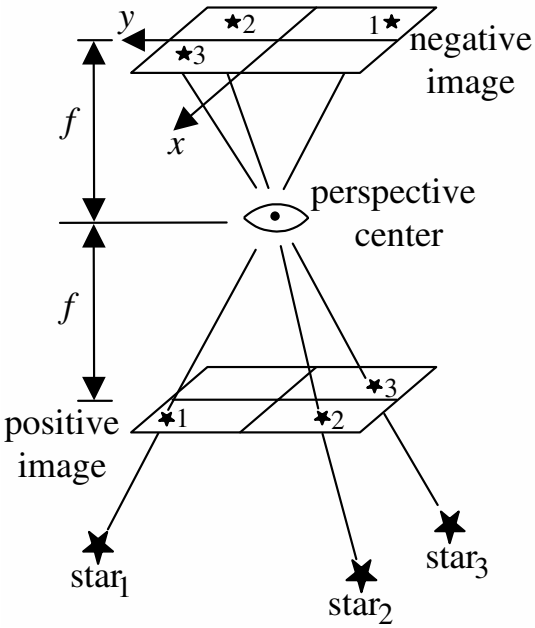

Figure 4.3: Collinearity of Perspective Center, Image, and Object

The measurement model in eqn. (4.11) is also valid for three-axis magnetometers and Earth-horizon sensors.

4.2.2 Maximum Likelihood Estimation

The maximum-likelihood approach for attitude estimation minimizes the following loss function:

$$\boxed{J(\hat{A}) = \frac{1}{2}\sum_{j=1}^{N} \sigma_j^{-2} \|\tilde{\mathbf{b}}_j - \hat{A}\mathbf{r}_j\|^2} \tag{4.13}$$

subject to the constraint

$$\hat{A}\hat{A}^T = I_{3\times 3} \tag{4.14}$$

This problem was first posed by Grace Wahba[8] in 1965. Although the least squares minimization in eqn. (4.13) seems to be straightforward, the equality constraint in eqn. (4.14) complicates the solution, which has lead to a wide area of linear algebra research for the computationally optimal solution since Wahba's original paper. Before proceeding with the solution to this problem, we first derive an estimate error covariance expression. This is accomplished by using results from maximum likelihood estimation of §2.4. Recall that the Fisher information matrix for a parameter

vector $\mathbf{x}$ is given by

$$F = E\left\{\frac{\partial}{\partial \mathbf{x}\,\partial \mathbf{x}^T} J(\mathbf{x})\right\} \tag{4.15}$$

where $J(\mathbf{x})$ is the negative log-likelihood function, which is the loss function in this case (neglecting terms independent of A). Asymptotically, the Fisher information matrix tends to the inverse of the estimate error covariance so that

$$\lim_{N\to\infty} F = P^{-1} \tag{4.16}$$

The Fisher information for the attitude is expressed in terms of incremental error angles, $\boldsymbol{\delta\alpha}$, defined according to

$$\hat{A} = e^{-[\boldsymbol{\delta\alpha}\times]} A \approx (I_{3\times 3} - [\boldsymbol{\delta\alpha}\times])\, A \tag{4.17}$$

where the 3×3 matrix $[\boldsymbol{\delta\alpha}\times]$ is a cross product matrix, see eqn. (3.149). Higher-order terms in the Taylor series expansion of the exponential function are not required since they do not contribute to the Fisher information matrix. The parameter vector is now given by $\mathbf{x} = \boldsymbol{\delta\alpha}$, and the covariance is defined by $P = E\left\{\mathbf{x}\mathbf{x}^T\right\} - E\{\mathbf{x}\}E^T\{\mathbf{x}\}$. Substituting eqn. (4.17) into eqn. (4.13), and after taking the appropriate partials the following optimal error covariance can be derived:

$$\boxed{P = \left(-\sum_{j=1}^{N} \sigma_j^{-2} [A\,\mathbf{r}_j\times]^2\right)^{-1}} \tag{4.18}$$

The attitude A is evaluated at its respective *true* value. In practice, though, $A\,\mathbf{r}_j$ is often replaced with the measurement $\tilde{\mathbf{b}}_j$, which allows a calculation of the covariance without computing an attitude! Equation (4.18) gives the Cramér-Rao lower bound (any estimator whose error covariance is equivalent to eqn. (4.18) is an *efficient*, i.e., optimal estimator). The Fisher information matrix is nonsingular only if at least two non-collinear observation vectors exist. This is due to the fact that one vector observation gives only two pieces of attitude information. To see this fact we first use the following identity:

$$-[A\,\mathbf{r}\times]^2 = ||\mathbf{r}||^2 I_{3\times 3} - (A\,\mathbf{r})(A\,\mathbf{r})^T \tag{4.19}$$

This matrix has rank 2 and is the projection operator (see §1.6.4) onto the space perpendicular to $A\,\mathbf{r}$, which reflects the fact that an observation of a vector contains no information about rotations around an axis specified by that vector.

4.2.3 Optimal Quaternion Solution

One approach to determine the attitude involves using the Euler angle parameterization of the attitude matrix, shown in §3.7.1. Nonlinear least squares may be employed to determine the Euler angles; however, this is a highly iterative approach

due to the nonlinear parameterization of the attitude matrix, which involve transcendental functions. A more elegant algorithm is given by Davenport, known as the *q-method*.[9] The loss function in eqn. (4.13) may be rewritten as

$$J(\hat{A}) = -\sum_{j=1}^{N} \sigma_j^{-2} \tilde{\mathbf{b}}_j^T \hat{A} \mathbf{r}_j + \text{constant terms} \tag{4.20}$$

This loss function is clearly a minimum when

$$J(\hat{A}) = \sum_{j=1}^{N} \sigma_j^{-2} \tilde{\mathbf{b}}_j^T \hat{A} \mathbf{r}_j \tag{4.21}$$

is a maximum (dropping the constant terms which are not needed). To determine the attitude we parameterize $\hat{A}$ in term of the quaternion using eqn. (3.154), so that eqn. (4.21) is rewritten as

$$J(\hat{\mathbf{q}}) = \sum_{j=1}^{N} \sigma_j^{-2} \tilde{\mathbf{b}}_j^T \Xi^T(\hat{\mathbf{q}}) \Psi(\hat{\mathbf{q}}) \mathbf{r}_j \tag{4.22}$$

Also, the orthogonality constraint in eqn. (4.14) reduces to $\hat{\mathbf{q}}^T \hat{\mathbf{q}} = 1$ for the quaternion. Using the identities in eqns. (3.161) and (3.164) leads to

$$J(\hat{\mathbf{q}}) = \hat{\mathbf{q}}^T K \hat{\mathbf{q}} \tag{4.23}$$

with

$$K \equiv -\sum_{j=1}^{N} \sigma_j^{-2} \Omega(\tilde{\mathbf{b}}_j) \Gamma(\mathbf{r}_j) \tag{4.24}$$

where $\Omega(\tilde{\mathbf{b}})$ and $\Gamma(\mathbf{r})$ are defined in eqns. (3.162) and (3.165), respectively. Note that these matrices commute so that $\Omega(\tilde{\mathbf{b}})\Gamma(\mathbf{r}) = \Gamma(\mathbf{r})\Omega(\tilde{\mathbf{b}})$. The extrema of $J(\hat{\mathbf{q}})$, subject to the normalization constraint $\hat{\mathbf{q}}^T \hat{\mathbf{q}} = 1$, is found by using the method of Lagrange multipliers (see Appendix C). The necessary conditions can be found by maximizing the following augmented function:

$$J(\hat{\mathbf{q}}) = \hat{\mathbf{q}}^T K \hat{\mathbf{q}} + \lambda(1 - \hat{\mathbf{q}}^T \hat{\mathbf{q}}) \tag{4.25}$$

where λ is a Lagrange multiplier. Therefore, as necessary conditions for constrained minimization of J, we have the following requirement:

$$\boxed{K\hat{\mathbf{q}} = \lambda \hat{\mathbf{q}}} \tag{4.26}$$

Equation (4.26) represents an eigenvalue decomposition of the matrix K, where the quaternion is an eigenvector of K and λ is an eigenvalue. Substituting eqn. (4.26) into eqn. (4.23) gives

$$J(\hat{\mathbf{q}}) = \lambda \tag{4.27}$$

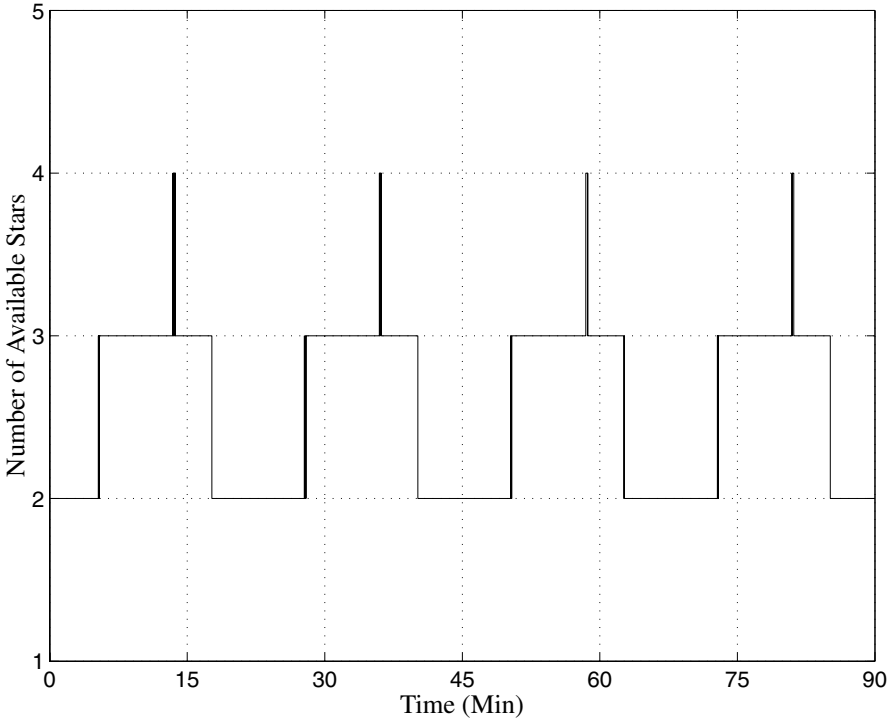

Figure 4.4: Availability of Stars

Thus, in order to maximize J the optimal quaternion $\hat{\mathbf{q}}$ is given by the eigenvector corresponding to the largest eigenvalue of K. It can be shown that if at least two non-collinear observation vectors exist, then the eigenvalues of K are distinct, which yields an unambiguous quaternion. Shuster[10] developed an algorithm, called QUEST (QUaternion ESTimator), that computes that quaternion without the necessity of performing an eigenvalue decomposition, which gives a very computationally efficient algorithm. This algorithm is widely used for many on-board spacecraft applications. Yet another efficient algorithm, developed by Mortari, called Estimator of Optimal Quaternion (ESOQ) is given in Ref. [11]. Also, Markley[12] develops an algorithm, using a singular value decomposition (SVD) approach, that determines the attitude matrix A directly.

Example 4.2: In this example a simulation using a typical star camera is used to determine the attitude of a rotating spacecraft. The star camera can sense up to 10 stars in a $6^\circ \times 6^\circ$ field-of-view. The catalog contains stars that can be sensed up to a magnitude of 5.0 (larger magnitudes indicate dimmer stars). The star camera's boresight is assumed to be along the z-axis pointed in the anti-nadir direction, and is initially aligned with the $\hat{\mathbf{r}}_1$ vector of the inertial reference frame shown in Figure

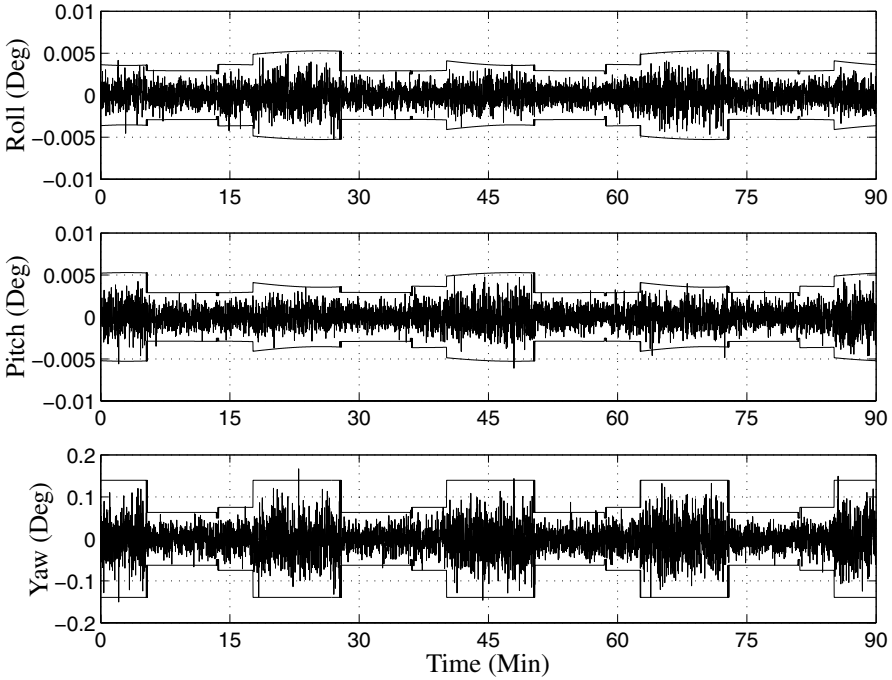

Figure 4.5: Attitude Errors and Boundaries

4.2. A rotation about the $\hat{\mathbf{r}}_3$ vector only is assumed and the spacecraft is in a 90-minute orbit (i.e., low Earth orbit). Star images are taken at 1-second intervals. A plot of the number of available stars over the full 360 degree rotation of the orbit is shown in Figure 4.4. The minimum number of available stars is two, which is also the minimum number required for attitude determination. In general, as the number of available stars decreases, the attitude accuracy degrades (although this is also dependent on the angle separation between stars). Generally, three or four stars are required for the first image, in order to reliably identify star patterns, associating each measured vector with the corresponding cataloged vector.

The star camera body observations are obtained by using eqn. (4.9), with an assumed focal length of 42.98 mm. Simulated measurements are derived using a zero-mean Gaussian noise process, which are added to the true values of x_j and y_j in eqn. (4.7):

$$\tilde{x}_j = x_j + v_{x_j}$$
$$\tilde{y}_j = y_j + v_{y_j}$$

where (v_{x_j}, v_{y_j}) are uncorrelated zero-mean Gaussian random variables each with a 3σ value of 0.005 degrees. We also assume that no sun obtrusions are present (although this is not truly realistic). At each time instant all available inertial star

vectors and body measurements are used to form the K matrix in eqn. (4.24). Then, the quaternion estimate is found using eqn. (4.26). Furthermore, the attitude error-covariance is computed using eqn. (4.18), and the diagonal elements of this matrix are used to form 3σ boundaries on the attitude errors. A plot of the attitude errors and associated 3σ boundaries is shown in Figure 4.5. Clearly, the computed 3σ boundaries do indeed bound the attitude errors. Note that the yaw errors are much larger than the roll and pitch errors. This is due to the fact that the boresight of the star camera is along this yaw rotation axis. Also, as expected, the accuracy degrades as the number of available stars decreases, which is also illustrated in the covariance matrix. This covariance analysis provides valuable information to assess the expected performance of the attitude determination process (which can be calculated without any attitude knowledge!). In Chapter 7, we shall see how the accuracy can be significantly improved using rate gyroscope measurements in a Kalman filter.

4.2.4 Information Matrix Analysis

In this section an analysis of the observable attitude axes using the information matrix is shown. This analysis is shown for one and two vector observations. For one-vector observation the information matrix, which is the inverse of eqn. (4.18), is given by

$$F = -\sigma^{-2}[\mathbf{b}\times]^2 \tag{4.28}$$

where $\mathbf{b} \equiv A\,\mathbf{r}$. An eigenvalue/eigenvector decomposition can be useful to assess the observability of this system. Since F is a symmetric positive semi-definite matrix, then all of its eigenvalues are greater than or equal to zero (see Appendix A). Furthermore, the matrix of eigenvectors is orthogonal, which can be used to define a coordinate system. The eigenvalues of this matrix are given by $\lambda_1 = 0$ and $\lambda_{2,3} = \sigma^{-2}\mathbf{b}^T\mathbf{b}$. This indicates that rotations about one of the eigenvectors is not observable. The eigenvector associated with the zero eigenvalue is along $\mathbf{b}/||\mathbf{b}||$. Therefore, rotations about the boresight of the body vector are unknown, which intuitively makes sense. The other observable axes are perpendicular to this unobservable axis, which also intuitively makes sense.

A more interesting case involves two vector observations. The information matrix for this case is given by

$$F = -\sigma_1^{-2}[\mathbf{b}_1\times]^2 - \sigma_2^{-2}[\mathbf{b}_2\times]^2 \tag{4.29}$$

where $\mathbf{b}_1 \equiv A\,\mathbf{r}_1$ and $\mathbf{b}_2 \equiv A\,\mathbf{r}_2$. For any vector, $\mathbf{a}$, the following identity is true: $-[\mathbf{a}\times]^2 = (\mathbf{a}^T\mathbf{a})I_{3\times3} - \mathbf{a}\,\mathbf{a}^T$. Using this identity simplifies eqn. (4.29) to

$$F = \sigma_1^{-2}\left[(\mathbf{b}_1^T\mathbf{b}_1)I_{3\times3} - \mathbf{b}_1\mathbf{b}_1^T\right] + \sigma_2^{-2}\left[(\mathbf{b}_2^T\mathbf{b}_2)I_{3\times3} - \mathbf{b}_2\mathbf{b}_2^T\right] \tag{4.30}$$

If two non-collinear vector observations exist, then the system is fully observable and no zero eigenvalues of F will exist. The maximum eigenvalue of F can be shown to

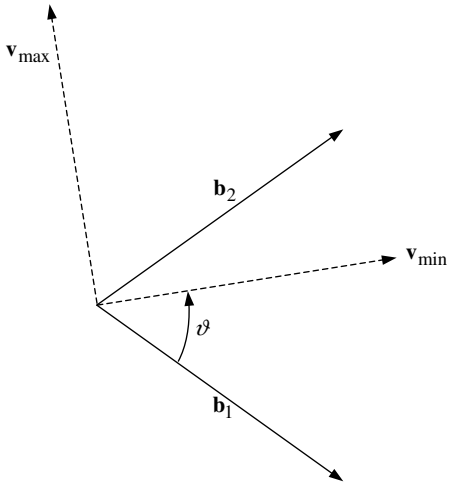

Figure 4.6: Observable Axes with Two Vector Observations

be given by

$$\lambda_{max} = \sigma_1^{-2}\mathbf{b}_1^T\mathbf{b}_1 + \sigma_2^{-2}\mathbf{b}_2^T\mathbf{b}_2 \tag{4.31}$$

Factoring this eigenvalue out of the characteristic equation, $|\lambda I_{3\times 3} - F|$, yields the following form for the remaining eigenvalues:

$$\lambda^2 - \lambda_{max}\lambda + \sigma_1^{-2}\sigma_2^{-2}||\mathbf{b}_1 \times \mathbf{b}_2||^2 = 0 \tag{4.32}$$

Therefore, the intermediate and minimum eigenvalues are given by

$$\lambda_{int} = \frac{\lambda_{max}(1+\chi)}{2} \tag{4.33a}$$

$$\lambda_{min} = \frac{\lambda_{max}(1-\chi)}{2} \tag{4.33b}$$

where

$$\chi = \left[\frac{\lambda_{max}^2 - 4\sigma_1^{-2}\sigma_2^{-2}||\mathbf{b}_1 \times \mathbf{b}_2||^2}{\lambda_{max}^2}\right]^{1/2} \tag{4.34}$$

Note that $\lambda_{max} = \lambda_{min} + \lambda_{int}$.

The eigenvectors of F are computed by solving $\lambda\mathbf{v} = F\mathbf{v}$ for each eigenvalue. The eigenvector associated with the maximum eigenvalue can be shown to be given by

$$\mathbf{v}_{max} = \pm\frac{\mathbf{b}_1 \times \mathbf{b}_2}{||\mathbf{b}_1 \times \mathbf{b}_2||} \tag{4.35}$$

The sign of this vector is not of consequence since we are only interested in rotations about this vector. This indicates that the most observable axis is perpendicular to the

plane formed by $\mathbf{b}_1$ and $\mathbf{b}_2$, which intuitively makes sense. The remaining eigenvectors must surely lie in the $\mathbf{b}_1$-$\mathbf{b}_2$ plane. To determine the eigenvector associated with the minimum eigenvalue, we will perform a rotation about the $\mathbf{v}_{\max}$ axis and determine the angle from $\mathbf{b}_1$. Using the Euler axis and angle parameterization in eqn. (3.151) gives

$$\mathbf{v}_{\min} = \pm \left\{ (\cos\vartheta) I_{3\times 3} + (1-\cos\vartheta)\mathbf{v}_{\max}\mathbf{v}_{\max}^T - \sin\vartheta [\mathbf{v}_{\max}\times] \right\} \frac{\mathbf{b}_1}{||\mathbf{b}_1||} \tag{4.36}$$

where ϑ is the angle used to rotate $\mathbf{b}_1/||\mathbf{b}_1||$ to $\mathbf{v}_{\min}$. Using the fact that $\mathbf{v}_{\max}$ is perpendicular to $\mathbf{b}_1$ gives $\mathbf{v}_{\max}^T\mathbf{b}_1 = 0$. Therefore, eqn. (4.36) reduces down to

$$\mathbf{v}_{\min} = \pm \{ (\cos\vartheta) I_{3\times 3} - \sin\vartheta [\mathbf{v}_{\max}\times] \} \frac{\mathbf{b}_1}{||\mathbf{b}_1||} \tag{4.37}$$

Substituting eqn. (4.37) into $\lambda_{\min}\mathbf{v}_{\min} = F\mathbf{v}_{\min}$ and using the property of the cross product matrix leads to the following equation for ϑ:

$$\tan\vartheta = \frac{a+b}{c} \tag{4.38}$$

where

$$a \equiv \lambda_{\min}\sigma_1^{-2}\mathbf{b}_1^T\mathbf{b}_1 \tag{4.39a}$$

$$b \equiv \sigma_1^{-2}\sigma_2^{-2}\mathbf{b}_1^T[\mathbf{b}_2\times]^2\mathbf{b}_1 \tag{4.39b}$$

$$c \equiv -\frac{\sigma_1^{-2}\sigma_2^{-2}\mathbf{b}_1^T[\mathbf{b}_2\times]^2[\mathbf{b}_1\times]^2\mathbf{b}_2}{||\mathbf{b}_1\times\mathbf{b}_2||} \tag{4.39c}$$

Equation (4.38) can now be solved for ϑ, which can be used to determine $\mathbf{v}_{\min}$ from eqns. (4.35) and (4.37). The intermediate axis is simply given by the cross product of $\mathbf{v}_{\max}$ and $\mathbf{v}_{\min}$:

$$\mathbf{v}_{\text{int}} = \pm\mathbf{v}_{\max}\times\mathbf{v}_{\min} \tag{4.40}$$

A plot of the minimum and intermediate axes is shown in Figure 4.6 for the case when the angle between $\mathbf{b}_1$ and $\mathbf{b}_2$ is less than 90 degrees. Intuitively, this analysis makes sense since we expect that the least determined axis, $\mathbf{v}_{\min}$, is somewhere *between* $\mathbf{b}_1$ and $\mathbf{b}_2$ if these vector observations are less than 90 degrees apart.

The previous analysis greatly simplifies if the reference vectors are unit vectors and the variances of each observation are equal, so that $\sigma_1^2 = \sigma_2^2 \equiv \sigma^2$. These assumptions are valid for a single field-of-view star camera. The eigenvalues are now given by

$$\lambda_{\max} = 2\sigma^{-2} \tag{4.41a}$$

$$\lambda_{\text{int}} = \sigma^{-2}(1+|\mathbf{b}_1^T\mathbf{b}_2|) \tag{4.41b}$$

$$\lambda_{\min} = \sigma^{-2}(1-|\mathbf{b}_1^T\mathbf{b}_2|) \tag{4.41c}$$

The eigenvectors are now given by

$$\mathbf{v}_{\max} = \pm \frac{\mathbf{b}_1 \times \mathbf{b}_2}{||\mathbf{b}_1 \times \mathbf{b}_2||} \tag{4.42a}$$

$$\mathbf{v}_{\text{int}} = \pm \frac{\mathbf{b}_1 - \text{sign}(\mathbf{b}_1^T \mathbf{b}_2)\mathbf{b}_2}{||\mathbf{b}_1 - \text{sign}(\mathbf{b}_1^T \mathbf{b}_2)\mathbf{b}_2||} \tag{4.42b}$$

$$\mathbf{v}_{\min} = \pm \frac{\mathbf{b}_1 + \text{sign}(\mathbf{b}_1^T \mathbf{b}_2)\mathbf{b}_2}{||\mathbf{b}_1 + \text{sign}(\mathbf{b}_1^T \mathbf{b}_2)\mathbf{b}_2||} \tag{4.42c}$$

where $\text{sign}(\mathbf{b}_1^T \mathbf{b}_2)$ is used to ensure that the proper direction of the eigenvectors is determined when the angle between $\mathbf{b}_1$ and $\mathbf{b}_2$ is greater than 90 degrees. If this angle is less than 90 degrees then $\mathbf{v}_{\min}$ is the *bisector* of $\mathbf{b}_1$ and $\mathbf{b}_2$. Intuitively this makes sense since we expect rotations perpendicular to the bisector of the two vector observations to be more observable than rotations about the bisector (again assuming that the vector observations are within 90 degrees of each other).

The analysis presented in this section is extremely useful for the visualization of the observability of the determined attitude. Closed-form solutions for special cases have been presented here. Still, in general, the eigenvalues and eigenvectors of the information matrix can be used to analyze the observability for cases involving multiple observations. An analytical observability analysis for a more complicated system is shown in Ref. [13].

4.3 Orbit Determination

In this section nonlinear least squares is used to determine the orbit of a spacecraft from range and line-of-sight (angle) observations. It is interesting to note that the original estimation problem motivating Gauss (i.e., determination of the planetary orbits from telescope/sextant observations) was nonlinear, and his methods (essentially §1.2) have survived as a standard operating procedure to this day.

Consider an observer (i.e., a radar site) that measures a range, azimuth, and elevation to a spacecraft in orbit. The geometry and common terminology associated with this observation is shown in Figure 4.7, where: $\boldsymbol{\rho}$ is the slant range, $\mathbf{r}$ is the radius vector locating the spacecraft, $\mathbf{R}$ is the radius vector locating the observer, α and δ is the right ascension and declination of the spacecraft, respectively, θ is the sidereal time of the observer, λ is the latitude of the observer, and ϕ is the east longitude from the observer to the spacecraft. The fundamental observation is given by

$$\boldsymbol{\rho} = \mathbf{r} - \mathbf{R} \tag{4.43}$$

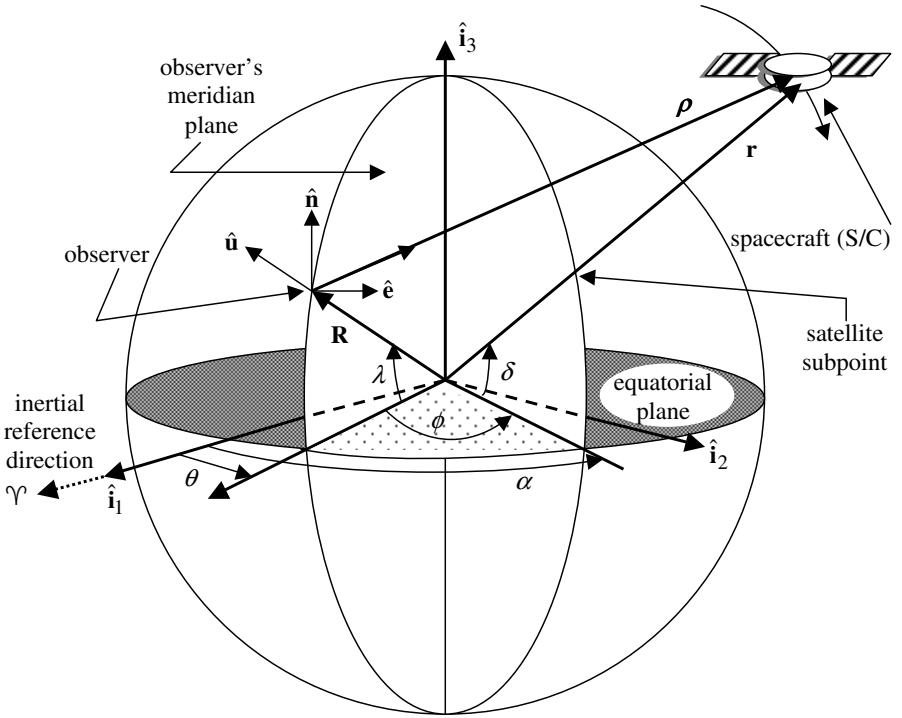

Figure 4.7: Geometry of Earth Observations of Spacecraft Motion

In non-rotating equatorial (inertial) components the vector $\boldsymbol{\rho}$ is given by

$$\boldsymbol{\rho} = \begin{bmatrix} x - ||\mathbf{R}|| \cos\lambda \cos\theta \\ y - ||\mathbf{R}|| \cos\lambda \sin\theta \\ z - ||\mathbf{R}|| \sin\lambda \end{bmatrix} \tag{4.44}$$

where x, y, and z are the components of the vector $\mathbf{r}$. The conversion from the inertial to the observer coordinate system ("up, east and north") is given by

$$\begin{bmatrix} \rho_u \\ \rho_e \\ \rho_n \end{bmatrix} = \begin{bmatrix} \cos\lambda & 0 & \sin\lambda \\ 0 & 1 & 0 \\ -\sin\lambda & 0 & \cos\lambda \end{bmatrix} \begin{bmatrix} \cos\theta & \sin\theta & 0 \\ -\sin\theta & \cos\theta & 0 \\ 0 & 0 & 1 \end{bmatrix} \boldsymbol{\rho} \tag{4.45}$$

Next, consider a radar site that measures the azimuth, az, elevation, el, and range, ρ. The observation equations are given by

$$\boxed{\begin{aligned} ||\boldsymbol{\rho}|| &= (\rho_u^2 + \rho_e^2 + \rho_n^2)^{1/2} && \text{(4.46a)} \\ \text{az} &= \tan^{-1}\left(\frac{\rho_e}{\rho_n}\right) && \text{(4.46b)} \\ \text{el} &= \sin^{-1}\left(\frac{\rho_u}{||\boldsymbol{\rho}||}\right) && \text{(4.46c)} \end{aligned}}$$

The basic two-body orbital equation of motion is given by (see §3.8.2)

$$\boxed{\ddot{\mathbf{r}} = -\frac{\mu}{||\mathbf{r}||^3}\mathbf{r}} \tag{4.47}$$

The goal of orbit determination is to determine initial conditions for the position and velocity of $\mathbf{x}_0 = \begin{bmatrix}\mathbf{r}_0^T & \dot{\mathbf{r}}_0^T\end{bmatrix}^T$ from the observations. The nonlinear least square differential correction algorithm for orbit determination is shown in Figure 4.8. The model equation is given by eqn. (4.47) with $\mathbf{x} = \begin{bmatrix}\mathbf{r}^T & \dot{\mathbf{r}}^T\end{bmatrix}^T$, and also includes other parameters if desired, given by $\mathbf{p}$ (e.g., the parameter μ can also be determined if desired). The measurement equation is given by eqn. (4.46) with $\mathbf{y} = \begin{bmatrix}||\boldsymbol{\rho}|| & \text{az} & \text{el}\end{bmatrix}^T$. Other quantities, such as measurement biases or force model parameters, can be appended to the measurement observation equation through the vector $\mathbf{b}$. The matrices $\Phi(t, t_0)$, $\Psi(t, t_0)$, F, and G are defined as

$$\Phi(t, t_0) \equiv \frac{\partial \mathbf{x}(t)}{\partial \mathbf{x}_0}, \quad \Psi(t, t_0) \equiv \frac{\partial \mathbf{x}(t)}{\partial \mathbf{p}} \tag{4.48a}$$

$$F \equiv \frac{\partial \mathbf{f}}{\partial \mathbf{x}}, \quad G \equiv \frac{\partial \mathbf{f}}{\partial \mathbf{p}} \tag{4.48b}$$

which are evaluated at the current estimates. The matrix H is computed using

$$H = \left[\frac{\partial \mathbf{h}}{\partial \mathbf{x}}\Phi(t, t_0) \;\; \frac{\partial \mathbf{h}}{\partial \mathbf{x}}\Psi(t, t_0) \;\; \frac{\partial \mathbf{h}}{\partial \mathbf{b}}\right] \tag{4.49}$$

which are again evaluated at the current estimates. Analytical expressions for $\Psi(t, t_0)$, F, and G are straightforward. The matrix F is given by

$$F = \begin{bmatrix} 0_{3\times 3} & I_{3\times 3} \\ F_{21} & 0_{3\times 3} \end{bmatrix} \tag{4.50}$$

where

$$F_{21} = \begin{bmatrix} \dfrac{3\mu x^2}{||\mathbf{r}||^5} - \dfrac{\mu}{||\mathbf{r}||^3} & \dfrac{3\mu xy}{||\mathbf{r}||^5} & \dfrac{3\mu xz}{||\mathbf{r}||^5} \\ \dfrac{3\mu xy}{||\mathbf{r}||^5} & \dfrac{3\mu y^2}{||\mathbf{r}||^5} - \dfrac{\mu}{||\mathbf{r}||^3} & \dfrac{3\mu yz}{||\mathbf{r}||^5} \\ \dfrac{3\mu xz}{||\mathbf{r}||^5} & \dfrac{3\mu yz}{||\mathbf{r}||^5} & \dfrac{3\mu z^2}{||\mathbf{r}||^5} - \dfrac{\mu}{||\mathbf{r}||^3} \end{bmatrix} \tag{4.51}$$

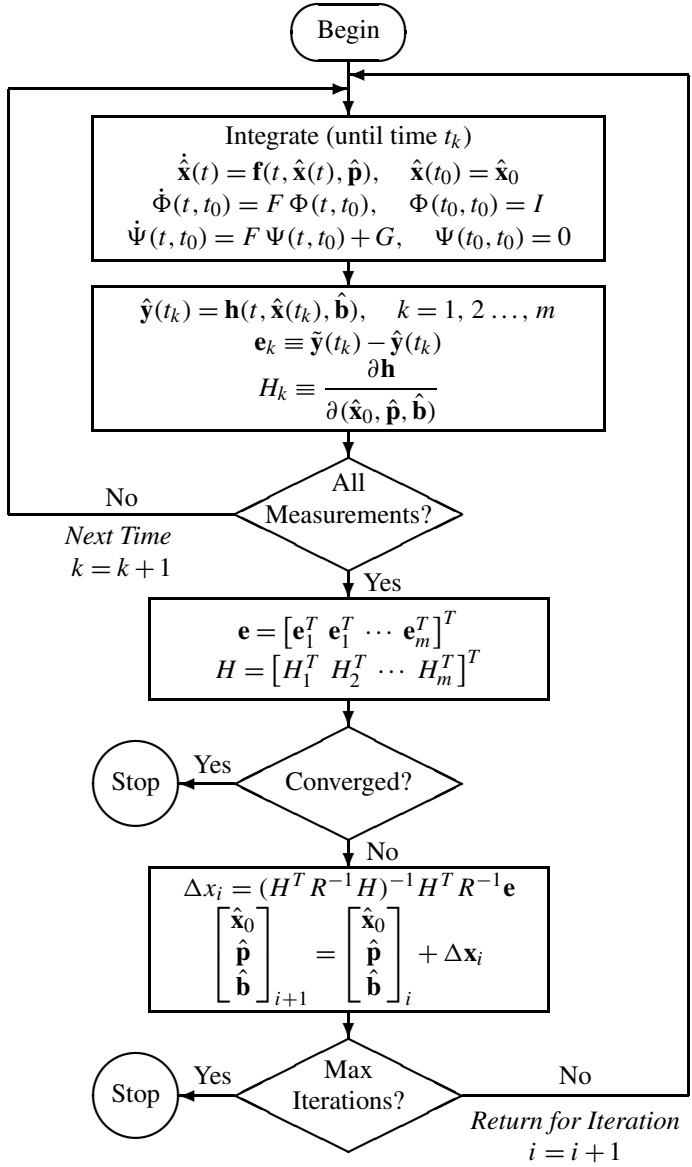

Figure 4.8: Least Squares Orbit Determination

For the general case of velocity dependent forces (such as drag), the lower right partition of eqn. (4.50) is nonzero. Analytical expressions for $\Phi(t, t_0)$ can be found in Refs. [14] and [15]. The "brute force" approach to determination of $\Phi(t, t_0)$ would be to attempt formal analytical or numerical solutions of the differential equation (3.88). However, we can make efficient use of the fact that the analytical solution is available

for $\mathbf{x}(t)$, for Keplerian motion, (see §3.8.2) to determine the desired solution for $\Phi(t, t_0)$ by partial differentiation of the equations. The appropriate equations for the partials are given by[14]

$$\Phi(t, t_0) = \begin{bmatrix} \Phi_{11} & \Phi_{12} \\ \Phi_{21} & \Phi_{22} \end{bmatrix} \tag{4.52}$$

where

$$\Phi_{11} = \frac{||\mathbf{r}||}{\mu}(\dot{\mathbf{r}} - \dot{\mathbf{r}}_0)(\dot{\mathbf{r}} - \dot{\mathbf{r}}_0)^T + ||\mathbf{r}_0||^{-3}[||\mathbf{r_0}||(1-f)\mathbf{r}\,\mathbf{r}_0^T + c\dot{\mathbf{r}}\,\mathbf{r}_0^T] + f I_{3\times 3} \tag{4.53a}$$

$$\Phi_{12} = \frac{||\mathbf{r}_0||}{\mu}(1-f)[(\mathbf{r} - \mathbf{r}_0)\dot{\mathbf{r}}_0^T - (\dot{\mathbf{r}} - \dot{\mathbf{r}}_0)\mathbf{r}_0^T] + \frac{c}{\mu}\dot{\mathbf{r}}\,\dot{\mathbf{r}}_0^T + g I_{3\times 3} \tag{4.53b}$$

$$\begin{aligned} \Phi_{21} = &-||\mathbf{r}_0||^{-2}(\dot{\mathbf{r}} - \dot{\mathbf{r}}_0)\mathbf{r}_0^T - ||\mathbf{r}||^{-2}\mathbf{r}(\dot{\mathbf{r}} - \dot{\mathbf{r}}_0)^T - \frac{\mu c}{||\mathbf{r}||^3||\mathbf{r}_0||^3}\mathbf{r}\,\mathbf{r}_0^T \\ &+ \dot{f}\left[I_{3\times 3} - ||\mathbf{r}_0||^{-2}\mathbf{r}\,\mathbf{r}^T + \frac{1}{\mu||\mathbf{r}||}(\mathbf{r}\,\dot{\mathbf{r}}^T - \dot{\mathbf{r}}\,\mathbf{r}^T)\mathbf{r}(\dot{\mathbf{r}} - \dot{\mathbf{r}}_0)^T\right] \end{aligned} \tag{4.53c}$$

$$\Phi_{22} = \frac{||\mathbf{r}_0||}{\mu}(\dot{\mathbf{r}} - \dot{\mathbf{r}}_0)(\dot{\mathbf{r}} - \dot{\mathbf{r}}_0)^T + ||\mathbf{r}_0||^{-3}[||\mathbf{r_0}||(1-f)\mathbf{r}\,\mathbf{r}_0^T - c\mathbf{r}\,\dot{\mathbf{r}}_0^T] + \dot{g} I_{3\times 3} \tag{4.53d}$$

The variables f, g, $\dot{f}$, and $\dot{g}$ are given in eqn. (3.201). The symbol c is defined by

$$c = (3u_5 - \chi u_4 - \sqrt{\mu}(t - t_0)u_2)/\sqrt{\mu} \tag{4.54}$$

where χ is a *generalized anomaly* given by

$$\chi = \alpha\sqrt{\mu}(t - t_0) + \frac{\mathbf{r}^T\dot{\mathbf{r}}}{\sqrt{\mu}} - \frac{\mathbf{r}_0^T\dot{\mathbf{r}}_0}{\sqrt{\mu}} \tag{4.55}$$

where $\alpha = 1/a$, which is given by eqn. (3.199), and the *universal functions* for elliptic orbits are given by

$$u_2 = \frac{1 - \cos(\sqrt{\alpha}\chi)}{\alpha} \tag{4.56a}$$

$$u_3 = \frac{\sqrt{\alpha}\chi - \sin(\sqrt{\alpha}\chi)}{\alpha\sqrt{\alpha}} \tag{4.56b}$$

$$u_4 = \frac{\chi^2}{2\alpha} - \frac{u_2}{\alpha} \tag{4.56c}$$

$$u_5 = \frac{\chi^3}{6\alpha} - \frac{u_3}{\alpha} \tag{4.56d}$$

Several interesting properties of the universal variables and functions $u_i(\alpha, \chi)$ can be found in Ref. [14], including universal algorithms to compute these functions for all species of two-body orbits. The partials for the observation, which are used to

form $\partial \mathbf{h}/\partial \mathbf{x}$, are given by

$$\frac{\partial ||\boldsymbol{\rho}||}{\partial x} = (\rho_u \cos\lambda \cos\theta - \rho_e \sin\theta - \rho_n \sin\lambda \cos\theta)/||\boldsymbol{\rho}|| \tag{4.57a}$$

$$\frac{\partial ||\boldsymbol{\rho}||}{\partial y} = (\rho_u \cos\lambda \sin\theta + \rho_e \cos\theta - \rho_n \sin\lambda \sin\theta)/||\boldsymbol{\rho}|| \tag{4.57b}$$

$$\frac{\partial ||\boldsymbol{\rho}||}{\partial z} = (\rho_u \sin\lambda + \rho_n \cos\lambda)/||\boldsymbol{\rho}|| \tag{4.57c}$$

$$\frac{\partial \mathrm{az}}{\partial x} = \frac{1}{(\rho_n^2 + \rho_e^2)}(\rho_e \sin\lambda \cos\theta - \rho_n \sin\theta) \tag{4.58a}$$

$$\frac{\partial \mathrm{az}}{\partial y} = \frac{1}{(\rho_n^2 + \rho_e^2)}(\rho_e \sin\lambda \sin\theta + \rho_n \cos\theta) \tag{4.58b}$$

$$\frac{\partial \mathrm{az}}{\partial z} = -\frac{1}{(\rho_n^2 + \rho_e^2)}\rho_e \cos\lambda \tag{4.58c}$$

$$\frac{\partial \mathrm{el}}{\partial x} = \frac{1}{||\boldsymbol{\rho}||(||\boldsymbol{\rho}||^2 - \rho_u^2)^{1/2}}\left(||\boldsymbol{\rho}|| \cos\lambda \cos\theta - \rho_u \frac{\partial ||\boldsymbol{\rho}||}{\partial x}\right) \tag{4.59a}$$

$$\frac{\partial \mathrm{el}}{\partial y} = \frac{1}{||\boldsymbol{\rho}||(||\boldsymbol{\rho}||^2 - \rho_u^2)^{1/2}}\left(||\boldsymbol{\rho}|| \cos\lambda \sin\theta - \rho_u \frac{\partial ||\boldsymbol{\rho}||}{\partial y}\right) \tag{4.59b}$$

$$\frac{\partial \mathrm{el}}{\partial z} = \frac{1}{||\boldsymbol{\rho}||(||\boldsymbol{\rho}||^2 - \rho_u^2)^{1/2}}\left(||\boldsymbol{\rho}|| \sin\lambda - \rho_u \frac{\partial ||\boldsymbol{\rho}||}{\partial z}\right) \tag{4.59c}$$

The matrix $\partial \mathbf{h}/\partial \mathbf{x}$ is given by

$$\frac{\partial \mathbf{h}}{\partial \mathbf{x}} = \begin{bmatrix} H_{11} & 0_{3\times 3} \end{bmatrix} \tag{4.60}$$

where

$$H_{11} = \begin{bmatrix} \dfrac{\partial ||\boldsymbol{\rho}||}{\partial x} & \dfrac{\partial ||\boldsymbol{\rho}||}{\partial y} & \dfrac{\partial ||\boldsymbol{\rho}||}{\partial z} \\ \dfrac{\partial \mathrm{az}}{\partial x} & \dfrac{\partial \mathrm{az}}{\partial y} & \dfrac{\partial \mathrm{az}}{\partial z} \\ \dfrac{\partial \mathrm{el}}{\partial x} & \dfrac{\partial \mathrm{el}}{\partial y} & \dfrac{\partial \mathrm{el}}{\partial z} \end{bmatrix} \tag{4.61}$$

The least square differential correction process for orbit determination is as follows: integrate the equations of motion and partial derivatives until the observation time (t_k); next, compute the measurement residual $\mathbf{e}_k$ and observation partial equation; if all measurements are processed then proceed, otherwise continue to the next observation time; then, check convergence and stop if the convergence criterion is

satisfied; otherwise, compute an updated correction and stop if the maximum number of iterations is given; continue the iteration process until a solution for the desired parameters is found.

Determining an initial estimate for the position and velocity is important to help achieve convergence (especially in the least squares approach). Several approaches exist for state determination from various sensor measurements (e.g., see Refs. [15] and [16]). We will show a popular approximate approach to determine the orbit given three observations of the range, azimuth, and elevation ($||\boldsymbol{\rho}||_k$, az_k, el_k, $k = 1, 2, 3$). Since $||\mathbf{R}||$, λ, and θ_k are known, then $\mathbf{R}_k$ can easily be computed by

$$\mathbf{R}_k = ||\mathbf{R}|| \begin{bmatrix} \cos\lambda\cos\theta_k \\ \cos\lambda\sin\theta_k \\ \sin\lambda \end{bmatrix} \quad k = 1, 2, 3 \tag{4.62}$$

Next compute

$$\boldsymbol{\rho}_k = \begin{bmatrix} \rho_u \\ \rho_e \\ \rho_n \end{bmatrix} = ||\boldsymbol{\rho}||_k \begin{bmatrix} \sin\text{el}_k \\ \cos\text{el}_k \sin\text{az}_k \\ \cos\text{el}_k \cos\text{az}_k \end{bmatrix} \quad k = 1, 2, 3 \tag{4.63}$$

The position is simply given by

$$\mathbf{r}_k = \begin{bmatrix} \cos\theta_k & -\sin\theta_k & 0 \\ \sin\theta_k & \cos\theta_k & 0 \\ 0 & 0 & 1 \end{bmatrix} \begin{bmatrix} \cos\lambda & 0 & -\sin\lambda \\ 0 & 1 & 0 \\ \sin\lambda & 0 & \cos\lambda \end{bmatrix} \boldsymbol{\rho}_k + \mathbf{R}_k \quad k = 1, 2, 3 \tag{4.64}$$

The velocity at second observation ($\dot{\mathbf{r}}_2$) can be determined from the three position vectors determined from eqn. (4.64). This is accomplished using a Taylor series expansion for the derivative. First, the following variables are computed:

$$\tau_{ij} = c\,(t_j - t_i) \tag{4.65a}$$

$$g_1 = \frac{\tau_{23}}{\tau_{12}\tau_{13}}, \quad g_3 = \frac{\tau_{12}}{\tau_{23}\tau_{13}}, \quad g_2 = g_1 - g_3 \tag{4.65b}$$

$$h_1 = \frac{\mu\tau_{23}}{12}, \quad h_3 = \frac{\mu\tau_{12}}{12}, \quad h_2 = h_1 - h_2 \tag{4.65c}$$

$$d_k = g_k + \frac{h_k}{||\mathbf{r}_k||^3}, \quad k = 1, 2, 3 \tag{4.65d}$$

where t_i and t_j are epoch times for $\mathbf{r}_i$ and $\mathbf{r}_j$, respectively, and $c = 1$, typically. The velocity is then given by[15]

$$\boxed{\dot{\mathbf{r}}_2 = -d_1\,\mathbf{r}_1 + d_2\,\mathbf{r}_2 + d_3\,\mathbf{r}_3} \tag{4.66}$$

This is known as the "Herrick-Gibbs" technique. The velocity is determined to within the order of $[(d^5||\mathbf{r}||/dt^5)/5!]\tau_{ij}^5$, which gives good results over short observation intervals. Typically, errors of a few kilometers in position and a few kilometers per second in velocity, for near Earth orbits, result in reliable convergence.

Example 4.3: In this example the least squares differential correction algorithm is used to determine the orbit of a spacecraft from range, azimuth, and elevation measurements. The true spacecraft position and velocity at epoch are given by

$$\mathbf{r}_0 = \begin{bmatrix} 7,000 & 1,000 & 200 \end{bmatrix}^T \text{ km}$$
$$\dot{\mathbf{r}}_0 = \begin{bmatrix} 4 & 7 & 2 \end{bmatrix}^T \text{ km/sec}$$

The latitude of the observer is given by $\lambda = 5°$, and the initial sidereal time is given by $\theta_0 = 10°$. Measurements are given at 10-second intervals over a 100-second simulation. The measurement errors are zero-mean Gaussian with a standard deviation of the range measurement error given by $\sigma_\rho = 1$ km, and a standard deviation of the angle measurements given by $\sigma_{\text{az}} = \sigma_{\text{el}} = 0.01°$. An initial estimate of the orbit parameters at the second time step is given by Herrick-Gibbs approach. The approximate results for position and velocity are given by

$$\hat{\mathbf{r}} = \begin{bmatrix} 7,038 & 1,070 & 221 \end{bmatrix}^T \text{ km}$$
$$\dot{\mathbf{r}} = \begin{bmatrix} 3.92 & 7.00 & 2.00 \end{bmatrix}^T \text{ km/sec}$$

The true position and velocity at the second time step are given by

$$\mathbf{r} = \begin{bmatrix} 7,040 & 1,070 & 220 \end{bmatrix}^T \text{ km}$$
$$\dot{\mathbf{r}} = \begin{bmatrix} 3.92 & 7.00 & 2.00 \end{bmatrix}^T \text{ km/sec}$$

which are in close agreement with the initial estimates. In order to assess the performance of the least squares differential correction algorithm the initial guesses for the position and velocity are given by $\hat{\mathbf{r}}_0 = \begin{bmatrix} 6,990 & 1 & 1 \end{bmatrix}^T$ km, and $\dot{\hat{\mathbf{r}}}_\mathbf{0} = \begin{bmatrix} 1 & 1 & 1 \end{bmatrix}^\mathbf{T}$ km/sec. Results for the least square iterations are given in Table 4.2. The algorithm converges after seven iterations, and does well for large initial condition errors (the Levenberg-Marquardt method of §1.6.3 may also be employed if needed). The 3σ bounds (determined using the diagonal elements of the estimate error-covariance) for position are $3\boldsymbol{\sigma}_{\hat{\mathbf{r}}} = \begin{bmatrix} 1.26 & 0.25 & 0.51 \end{bmatrix}^T$ km, and for velocity are $3\boldsymbol{\sigma}_{\dot{\hat{\mathbf{r}}}} = \begin{bmatrix} 0.020 & 0.008 & 0.006 \end{bmatrix}^T$ km/sec. The bounds are useful to predict the performance of the algorithms.

A powerful technology for precise orbit determination is GPS. Differential GPS provides extremely accurate orbit estimates. The accuracy of GPS derived estimates ultimately depends on the orbit of the spacecraft and the geometry of the available GPS satellite in view of the spacecraft. More details on orbit determination using GPS can be found in Ref. [17].

Table 4.2: Least Squares Iterations for Orbit Determination

Iteration	Position (km)			Velocity (km/sec)		
0	6,990	1	1	1	1	1
1	7,496	1,329	-178	5.30	6.20	-18.42
2	7,183	609	27	12.66	22.63	12.69
3	6,842	905	490	6.65	13.73	-8.15
4	6,795	963	255	9.33	7.38	1.36
5	6,985	989	199	4.24	7.20	1.89
6	7,000	1,000	200	4.00	7.00	2.00
7	7,000	1,000	200	4.00	7.00	2.00

4.4 Aircraft Parameter Identification

For aircraft dynamics, parameter identification of unknown aerodynamic coefficients or stability and control derivatives is useful to quantify the performance of a particular aircraft using dynamic models introduced in §3.9. These models are often used to design control systems to provide increased maneuverability and for use in the design of automated unpiloted vehicles. In general, these coefficients are usually first determined using wind tunnel applications, and, as a newer approach, using computational fluid dynamics. Parameter identification using flight measurement data is useful to provide a final verification of these coefficients, and also update models for other applications such as adaptive control algorithms. This section introduces the basic concepts which incorporate estimation principles for aircraft parameter identification from flight data. For the interested reader, a more detailed discussion is given in Ref. [18].

Application of identification methods for aircraft coefficients dates back to the early 1920s, which involved basic detection of damping ratios and frequencies. In the 1940s and early 1950s these coefficients were fitted to frequency response data (magnitude and phase). Around the same time, linear least squares was applied using flight data, but gave poor results in the presence of measurement noise and gave biased estimates. Other methods, such as time vector techniques and analog matching methods, are described in Ref. [18]. The most popular approaches today for aircraft coefficient identification are based on maximum likelihood techniques as introduced in §2.3. The desirable attributes of these techniques, such as asymptotically unbiased and consistent estimates, are especially useful for the estimation of aircraft coefficients in the presence of measurement errors associated with flight data.

The aircraft equations of motion, derived in §3.9, can be written in continuous-discrete form as

$$\dot{\mathbf{x}} = \mathbf{f}(t, \mathbf{x}, \mathbf{p}) \tag{4.67a}$$

$$\tilde{\mathbf{y}}_k = \mathbf{h}(t_k, \mathbf{x}_k) + \mathbf{v}_k \tag{4.67b}$$

where $\mathbf{x}$ is the $n \times 1$ state vector (e.g., angle of attack, pitch angle, body rates, etc.), $\mathbf{p}$ is the $q \times 1$ vector of aircraft coefficients to be determined, $\mathbf{y}$ is the $m \times 1$ measurement vector, and $\mathbf{v}$ is the $m \times 1$ measurement-error vector which is assumed to be represented by a zero-mean Gaussian noise process with covariance R. Note that there is no noise associated with the state vector model. This will be addressed later in the Kalman filter of §5.3. Modelling errors may also be present, which lead to several obvious complications. However, the most common approach is to ignore it; any modelling error is most often treated as state or measurement noise, or both, in spite of the fact that the modelling error may be predominately deterministic rather than random.[18]

The maximum likelihood estimation approach minimizes the following loss function:

$$\boxed{J(\hat{\mathbf{p}}) = \frac{1}{2}\sum_{k=1}^{N}(\tilde{\mathbf{y}}_k - \hat{\mathbf{y}}_k)^T R^{-1}(\tilde{\mathbf{y}}_k - \hat{\mathbf{y}}_k)} \tag{4.68}$$

where $\hat{\mathbf{y}}_k$ is the estimated response of $\mathbf{y}$ at time t_k for a given value of the unknown parameter vector $\mathbf{p}$, and N is the total number of measurements. A common approach to minimize eqn. (4.68) for aircraft parameter identification involves using the Newton-Raphson algorithm. If i is the iteration number, then the $i+1$ estimate of $\mathbf{p}$, denoted by $\hat{\mathbf{p}}$, is obtained from the i^{th} estimate by[18]

$$\boxed{\hat{\mathbf{p}}_{i+1} = \hat{\mathbf{p}}_i - [\nabla^2_{\hat{\mathbf{p}}} J(\hat{\mathbf{p}})]^{-1}[\nabla_{\hat{\mathbf{p}}} J(\hat{\mathbf{p}})]} \tag{4.69}$$

where the first and second gradients are defined as

$$[\nabla_{\hat{\mathbf{p}}} J(\hat{\mathbf{p}})] = -\sum_{k=1}^{N}[\nabla_{\hat{\mathbf{p}}}\hat{\mathbf{y}}_k]^T R^{-1}(\tilde{\mathbf{y}}_k - \hat{\mathbf{y}}_k) \tag{4.70a}$$

$$[\nabla^2_{\hat{\mathbf{p}}} J(\hat{\mathbf{p}})] = \sum_{k=1}^{N}[\nabla_{\hat{\mathbf{p}}}\hat{\mathbf{y}}_k]^T R^{-1}[\nabla_{\hat{\mathbf{p}}}\hat{\mathbf{y}}_k] - \sum_{k=1}^{N}[\nabla^2_{\hat{\mathbf{p}}}\hat{\mathbf{y}}_k]R^{-1}(\tilde{\mathbf{y}}_k - \hat{\mathbf{y}}_k) \tag{4.70b}$$

The Gauss-Newton approximation to the second gradient is given by

$$[\nabla^2_{\hat{\mathbf{p}}} J(\hat{\mathbf{p}})] \approx \sum_{k=1}^{N}[\nabla_{\hat{\mathbf{p}}}\hat{\mathbf{y}}_k]^T R^{-1}[\nabla_{\hat{\mathbf{p}}}\hat{\mathbf{y}}_k] \tag{4.71}$$

This approximation is easier to compute than eqn. (4.70b), and has the advantage of possible decreased convergence time.

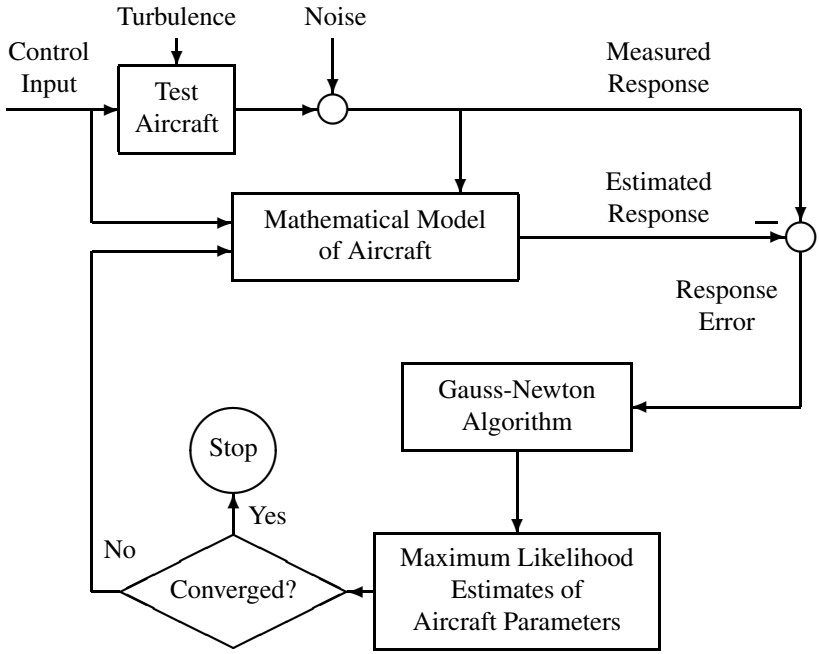

Figure 4.9: Aircraft Parameter Identification

The aircraft parameter identification process using maximum-likelihood is depicted in Figure 4.9.[18] First a control input is introduced to excite the motion. This input should be "rich" enough so that the test aircraft undergoes a general motion to allow sufficient observability of the to-be-identified parameters. For most applications, it is assumed that the control system inputs sufficiently dominate the motion in comparison to the effects of the turbulence and other unknown disturbances. An estimated response from the mathematical model is computed first using some initial guess of the aircraft parameters, which are usually obtained from ground-based wind tunnel data or by other means. A response error is computed from the estimated response and measured response. Then eqns. (4.69), (4.70a), and (4.71) are used to provide a Gauss-Newton update of the aircraft parameters. Next, the convergence is checked using some stopping criterion, e.g., eqn. (1.98). If the procedure has not converged then the previous aircraft parameters are replaced with the newly computed ones. These newly obtained aircraft parameters are used to compute a new estimated response from the mathematical model. The process continues until convergence is achieved. The error-covariance of the estimated parameters is given by the inverse of eqn. (4.71), which is also equivalent to within first-order terms to the Cramér-Rao lower bound.[18] Experiments are frequently repeated to confirm consistency. If the results are found to be consistent, then the measurements can be combined to obtain improved estimates.

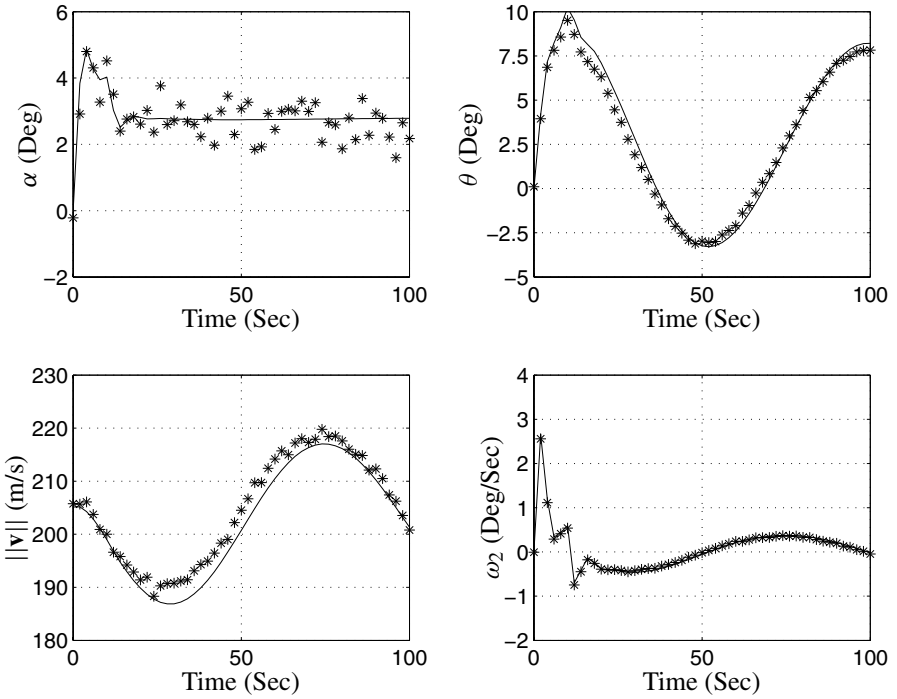

Figure 4.10: Simulated Aircraft Measurements and Estimated Trajectories

---

Example 4.4: To illustrate the power of maximum likelihood estimation, we show an example of identifying the longitudinal parameters of a simulated 747 aircraft. Decoupling the longitudinal motion equations from the lateral motion equations gives

$$\alpha = \tan^{-1}\frac{v_3}{v_1}$$
$$||\mathbf{v}|| = (v_1^2 + v_3^2)^{1/2}$$

$$T_1 - D\cos\alpha + L\sin\alpha - mg\sin\theta = m(\dot{v}_1 + v_3\omega_2)$$
$$T_3 - D\sin\alpha - L\cos\alpha + mg\cos\theta = m(\dot{v}_3 - v_1\omega_2)$$

$$D = C_D\,\bar{q}\,S$$
$$L = C_L\,\bar{q}\,S$$

$$\bar{q} = \frac{1}{2}\rho||\mathbf{v}||^2$$

$$C_D = C_{D_0} + C_{D_\alpha}\alpha + C_{D_{\delta_E}}\delta_E$$
$$C_L = C_{L_0} + C_{L_\alpha}\alpha + C_{L_{\delta_E}}\delta_E$$
$$J_{22}\dot{\omega}_2 = L_{A_2} + L_{T_2}$$
$$L_{A_2} = C_m \bar{q}\, S\, \bar{c}$$
$$C_m = C_{m_0} + C_{m_\alpha}\alpha + C_{m_{\delta_E}}\delta_E + C_{m_q}\frac{\omega_2 \bar{c}}{2||\mathbf{v}||^2}$$
$$\begin{bmatrix} \dot{x} \\ \dot{z} \end{bmatrix} = \begin{bmatrix} \cos\theta & \sin\theta \\ -\sin\theta & \cos\theta \end{bmatrix} \begin{bmatrix} v_1 \\ v_3 \end{bmatrix}$$
$$\dot{\theta} = \omega_2$$

The longitudinal aerodynamic coefficients, assuming a low cruise, for the 747 are given by

$$C_{D_0} = 0.0164 \quad C_{D_\alpha} = 0.20 \quad C_{D_{\delta_E}} = 0$$
$$C_{L_0} = 0.21 \quad C_{L_\alpha} = 4.4 \quad C_{L_{\delta_E}} = 0.32$$
$$C_{m_0} = 0 \quad C_{m_\alpha} = -1.00 \quad C_{m_{\delta_E}} = -1.30 \quad C_{m_q} = -20.5$$

The reference geometry quantities and density are given by

$$S = 510.97\,\text{m}^2 \quad \bar{c} = 8.321\,\text{m} \quad b = 59.74\,\text{m} \quad \rho = 0.6536033\,\text{kg/m}^3$$

The mass data and inertia quantities are given by

$$m = 288,674.58\,\text{kg} \qquad J_{22} = 44,877,565\,\text{kg m}^2$$

The flight conditions for low cruise at an altitude of 6,096 m are given by

$$||\mathbf{v}|| = 205.13\,\text{m/s} \quad \bar{q} = 13,751.2\,\text{N/m}^2$$

Using these flight conditions the equations of motion are integrated for a 100-second simulation. The thrust is set equal to the computed drag, and the elevator is set to 1 degree down from the trim value for the first 10 seconds and then returned to the trimmed value thereafter. Measurements of angle of attack, α, pitch angle, θ, velocity, $||\mathbf{v}||$, and angular velocity, ω_2, are assumed with standard deviations of the measurement errors given by $\sigma_\alpha = 0.5$ degrees, $\sigma_\theta = 0.1$ degrees, $\sigma_{||\mathbf{v}||} = 1$ m/s, and $\sigma_{\omega_2} = 0.01$ deg/sec, respectively. A plot of the simulated measurements is shown in Figure 4.10. Clearly, the angle of attack measurements are very noisy due to the inaccuracy of the sensor. The quantities to be estimated are given by

$$\mathbf{p} = [C_{D_0}\ C_{L_0}\ C_{m_0}\ C_{D_\alpha}\ C_{L_\alpha}\ C_{m_\alpha}]^T$$

The initial guesses for these parameters are given by

$$C_{D_0} = 0.01 \quad C_{L_0} = 0.1 \quad C_{m_0} = 0.01$$
$$C_{D_\alpha} = 0.30 \quad C_{L_\alpha} = 3 \quad C_{m_\alpha} = -0.5$$

which represent a significant departure from the actual values. The partial derivatives used in the Gauss-Newton algorithms are computed using a simple first-order numerical derivative, for example:

$$\frac{\partial \alpha}{\partial C_{D_0}} \approx \frac{\alpha|_{C_{D_0}+\delta C_{D_0}} - \alpha|_{C_{D_0}}}{\delta C_{D_0}}$$

Results of the convergence history are summarized below.

Iteration	Aircraft Parameter					
	C_{D_0}	C_{L_0}	C_{m_0}	C_{D_α}	C_{L_α}	C_{m_α}
0	0.0100	0.1000	0.0100	0.3000	3.0000	−0.5000
1	−0.0191	0.4185	−0.0432	0.5215	2.7383	−0.4932
2	0.0113	0.3755	−0.0404	0.0125	2.9932	−0.5603
3	0.0117	0.3528	−0.0342	0.2809	3.4661	−0.6835
4	0.0104	0.2954	−0.0221	0.3029	4.1408	−0.8554
5	0.0146	0.2167	−0.0033	0.1965	4.5201	−1.0213
6	0.0167	0.2057	0.0012	0.1938	4.3779	−1.0035
7	0.0163	0.2070	0.0007	0.2026	4.4064	−1.0025
8	0.0164	0.2069	0.0007	0.2004	4.4038	−1.0027
9	0.0164	0.2069	0.0007	0.2006	4.4041	−1.0026
10	0.0164	0.2069	0.0007	0.2006	4.4041	−1.0026

The 3σ error bounds, derived from the inverse of eqn. (4.71), are given by

	Aircraft Parameter					
	C_{D_0}	C_{L_0}	C_{m_0}	C_{D_α}	C_{L_α}	C_{m_α}
3σ	0.0025	0.0070	0.0021	0.0515	0.0545	0.0104

The estimate errors are clearly within the 3σ values. A plot of the estimated trajectories using the converged values are also shown in Figure 4.10. The velocity estimated trajectory seems to be biased slightly. This is due to the fact that the long period motion (known as the *phugoid* mode) seen in pitch and linear velocity is not well excited by elevator inputs. A speed brake is commonly used to fully excite the phugoid mode. Also, some parameters can be estimated more accurately than others (see Ref. [19] for details).

This section introduced the basic concepts of aircraft parameter identification. As demonstrated here, the maximum likelihood technique is extremely useful to extract aircraft parameters from flight data. This approach has been used successfully for many years for a wide variety of aircraft ranging from transport vehicles to highly

maneuverable aircraft. Although the example shown in this section is highly simplified it does capture the essence of all aircraft parameter identification approaches. The reader is highly encouraged to pursue actual applications in the references cited here and in the open literature.

4.5 Eigensystem Realization Algorithm

Experimental modelling of systems is required for both the design of control laws and the quantification of actual system performance. Modelling of linear systems can be divided into two categories: 1) realization of system model and order, and 2) identification of actual system parameters. Either approach can be used to develop mathematical models that reconstruct the input/output behavior of the actual system. However, identification is inherently more complex since actual model parameters are sought (e.g., stability derivatives of an aircraft as demonstrated in §4.4), while realization generates non-physical representations of a particular system.

The realization of system models can be achieved in either the time domain or frequency domain. Frequency domain methods are inherently robust with respect to noise sensitivity, but typically require extensive computation. Also, these methods generally require insight on model form. Time domain methods generally do not require *a priori* knowledge of system form, but may be sensitive to measurement noise. A few time-domain algorithms of particular interest include: AutoRegressive Moving Average (ARMA) models,[20] Least Squares algorithms,[21] the Impulse Response technique,[22] and Ibrahim's Time Domain technique.[23] The Eigensystem Realization Algorithm[24] (ERA) expands upon these algorithms by utilizing singular value decompositions in the least squares process. The advantages of the ERA over other algorithms include: 1) the realizations have matrices that are internally balanced (i.e., equivalent controllability and observability Grammians), 2) repeated eigenvalues are identifiable, and 3) the order of the system can be estimated from the singular values computed in the ERA.

The majority of time domain methods are based on discrete difference equations. These equations are used since general input/output histories can be represented as a linear function of the sampling interval and system matrices. Discrete realizations from input/output data can be found if the input persistently excites the dynamics of the system. The realization of system models can be performed from a number of time input histories, including: free response data, impulse response data, and random response data. A majority of the time domain techniques rely on impulse response data, which leads to the *Markov parameters*. These parameters can be obtained by applying a Fast Fourier Transform (FFT) and an inverse FFT of a random input and output response data set, or by time-domain techniques.[25]

The ERA is derived by using the discrete-time dynamic model in eqn. (4.72):

$$\mathbf{x}_{k+1} = \Phi\,\mathbf{x}_k + \Gamma\,\mathbf{u}_k \tag{4.72a}$$

$$\mathbf{y}_k = H\,\mathbf{x}_k + D\,\mathbf{u}_k \tag{4.72b}$$

where $\mathbf{x}$ is an $n \times 1$ state vector, $\mathbf{u}$ is a $p \times 1$ input vector, and $\mathbf{y}$ is an $m \times 1$ output vector. Consider the SISO system with an impulse input for u_k (i.e., $u_0 = 1$ and $u_k = 0$ for $k \geq 1$) and zero initial state conditions. The evolution of the output proceeds as

$$y_0 = D \tag{4.73}$$

$$y_1 = H\Gamma \tag{4.74}$$

$$y_2 = H\Phi\Gamma \tag{4.75}$$

$$y_3 = H\Phi^2\Gamma \tag{4.76}$$

$$\vdots \tag{4.77}$$

$$y_k = H\Phi^{k-1}\Gamma \tag{4.78}$$

Clearly a pattern has been established. For the MIMO system the pattern is identical, which leads to the following discrete Markov parameters:

$$Y_0 = D \tag{4.79a}$$

$$Y_k = H\Phi^{k-1}\Gamma, \quad k \geq 1 \tag{4.79b}$$

The first step in the ERA is to form a $(r \times s)$ block *Hankel matrix* composed of impulse response data:

$$\mathcal{H}_{k-1} = \begin{bmatrix} Y_k & Y_{k+m_1} & \cdots & Y_{k+m_{s-1}} \\ Y_{k+l_1} & Y_{k+l_1+m_1} & \cdots & Y_{k+l_1+m_{s-1}} \\ \vdots & \vdots & \ddots & \vdots \\ Y_{k+l_{r-1}} & Y_{k+l_{r-1}+m_1} & \cdots & Y_{k+l_{r-1}+m_{s-1}} \end{bmatrix} \tag{4.80}$$

where r and s are arbitrary integers satisfying the inequalities $rm \geq n$ and $sp \geq n$, and l_i $(i = 1, 2, \ldots, r-1)$ and m_j $(j = 1, 2, \ldots, s-1)$ are arbitrary integers. The k^{th} order Hankel matrix can be shown to be given by

$$\mathcal{H}_k = V_r\,\Phi^k\,W_s \tag{4.81}$$

where

$$V_r = \begin{bmatrix} H \\ H\Phi^{l_1} \\ \vdots \\ H\Phi^{l_{r-1}} \end{bmatrix} \tag{4.82a}$$

$$W_s = \begin{bmatrix} \Gamma & \Phi^{m_1}\Gamma & \cdots & \Phi^{m_{s-1}}\Gamma \end{bmatrix} \tag{4.82b}$$

The matrices V_r and W_s are generalized observability and controllability matrices, respectively. The ERA is derived by using a singular value decomposition of $\mathcal{H}_0$, expressed as

$$\mathcal{H}_0 = P\,S\,Q^T \tag{4.83}$$

where P and Q are isometric matrices (i.e., all columns are orthonormal), with dimensions $rm \times n$ and $ps \times n$, respectively. Next, let $V_r = P\,S^{1/2}$ and $W_s = S^{1/2}Q^T$. For the equality $\mathcal{H}_1 = V_r \Phi W_s$ we now have

$$\mathcal{H}_1 = P\,S^{1/2}\Phi S^{1/2}Q^T \tag{4.84}$$

Next, we multiply the left-hand side of eqn. (4.84) by P^T and the right-hand side by Q. Therefore, since $P^T P = I$ and $Q^T Q = I$, and from the definitions of V_r and W_s we obtain the following system realization:

$$\boxed{\begin{aligned} \Phi &= S^{-1/2}P^T\mathcal{H}_1 Q\,S^{-1/2} && \text{(4.85a)}\\ \Gamma &= S^{1/2}Q^T E_p && \text{(4.85b)}\\ H &= E_m^T P\,S^{1/2} && \text{(4.85c)}\\ D &= Y_0 && \text{(4.85d)} \end{aligned}}$$

where $E_m^T = [I_{m\times m},\ 0_{m\times m}, \ldots, 0_{m\times m}]$ and $E_p^T = [I_{p\times p},\ 0_{p\times p}, \ldots, 0_{p\times p}]$. The ERA is in fact a least squares minimization (see Ref. [24] for details).

The order of the system can be estimated by examining the magnitude of the singular values of the Hankel matrix. These singular values, with diagonal elements s_i, are arranged as

$$s_1 \geq s_2 \geq \cdots \geq s_n \geq s_{n+1} \geq \cdots \geq s_N \tag{4.86}$$

where N is the total number of singular values. However, the presence of noise often produces an indeterministic value for n. Subsequently, a cutoff magnitude is chosen below which the singular values are assumed to be in the bandwidth of the noise. Juang and Pappa[26] studied effects of noise on the ERA for the case of zero-mean Gaussian measurement errors. A suitable region for the rank of the Hankel matrix can be determined by $s_i^2 > 2N\sigma^2$ for $i = 1, 2, \ldots, n$, where σ is the standard deviation of the measurement error. Hence, a realization of order n is possible using this rank test scheme.

The natural frequencies and damping ratios of the continuous-time system are determined by first calculating the eigenvalue matrix Λ_d and eigenvector matrix Ψ_d of the realized discrete-time state matrix Φ, with

$$\Psi_d^{-1}[S^{-1/2}P^T\mathcal{H}_1 Q\,S^{-1/2}]\Psi_d = \Lambda_d \tag{4.87}$$

The modal damping ratios and damped natural frequencies are then calculated by observing the real and imaginary parts of the eigenvalues, after a transformation from the z-plane to the s-plane is completed:

$$s_i = \frac{[\ln(\lambda_i) + 2\pi j]}{\Delta t} \tag{4.88}$$

where λ_i corresponds to the i^{th} eigenvalue of the matrix Λ_d, j corresponds to the imaginary component $\sqrt{-1}$, and Δt is the sampling interval. Although the eigenvalues and eigenvectors of the discrete-time system are usually complex, the transformation to the continuous-time domain can be performed by using a real algorithm since the realized state matrix has independent eigenvectors.[24]

The presence of random noise on the output measurements leads to a Hankel matrix that has a rank larger than the order of the system. The Modal Amplitude Coherence[24] (MAC) is used to estimate the degree of modal excitation (controllability) of each identified mode. Therefore, the MAC can be used to help distinguish the system modes from modes identified due to adverse noise effects or nonlinearities in the system. The MAC is defined as the coherence between the modal amplitude history and an ideal history formed by extrapolating the initial value of the history using the identified eigenvalue. The derivation begins by expressing the control input matrix and modal time history as

$$\Psi_d^{-1} S^{1/2} Q^T E_p = [\mathbf{b}_1, \mathbf{b}_2, \ldots, \mathbf{b}_n]^* \tag{4.89a}$$

$$\Psi_d^{-1} S^{1/2} Q^T = [\mathbf{q}_1, \mathbf{q}_2, \ldots, \mathbf{q}_n]^* \tag{4.89b}$$

where the asterisk is defined as the transpose complex conjugate, $\mathbf{b}_j$ is a column vector corresponding to the system eigenvalue s_j ($j = 1, 2, \ldots, n$), and $\mathbf{q}_j$ represents the modal time history from the real measurement data obtained by the decomposition of the Hankel matrix. Equation (4.89) is used to form a sequence of idealized modal amplitudes in the complex domain, represented by

$$\bar{\mathbf{q}}_j^* = [\mathbf{b}_j^*, \exp(t\,\Delta t\, s_j)\mathbf{b}_j^*, \ldots, \exp(t_{s-1}\,\Delta t\, s_j)\mathbf{b}_j^*] \tag{4.90}$$

where t_j is the j^{th} time shift defined in the Hankel matrix, and Δt is the sampling interval. The MAC coherence factor for the j^{th} mode can be determined from

$$\boxed{\gamma_j = \frac{|\bar{\mathbf{q}}_j^* \mathbf{q}_j|}{\left(|\bar{\mathbf{q}}_j^* \bar{\mathbf{q}}_j||\mathbf{q}_j^* \mathbf{q}_j|\right)^{1/2}}} \tag{4.91}$$

The MAC factor must have a range between 0 and 1. As this factor approaches 1, the initial modal amplitude and realized eigenvalues approach the true values for the j^{th} mode of the system. Conversely, a lower MAC factor indicates that the mode is not excited well during the testing procedure or is probably due to noise effects. Another factor, known as the Modal Phase Collinearity (MPC) can be used to indicate if the behavior of the identified modes exhibit normal mode characteristics (see Ref. [24] for details).

For vibratory systems, described in §3.10, determining the mass (M), stiffness (K), and damping (C) matrices is of interest. These matrices can be extracted from the realized system model given by the ERA. The MIMO state-space model considered for this process is assumed to be given by

$$\dot{\mathbf{x}} = \begin{bmatrix} 0 & I \\ -M^{-1}K & -M^{-1}C \end{bmatrix} \mathbf{x} + \begin{bmatrix} 0 \\ M^{-1} \end{bmatrix} \mathbf{u} \equiv F\mathbf{x} + B\mathbf{u} \tag{4.92a}$$

$$\mathbf{y} = \begin{bmatrix} I & 0 \end{bmatrix} \mathbf{x} \equiv H\mathbf{x} \tag{4.92b}$$

with obvious definitions for F, B, and H. The corresponding transfer function matrix from $\mathbf{u}$ to $\mathbf{y}$ is given by

$$H[sI - F]^{-1} B = [Ms^2 + Cs + K]^{-1} \equiv \Phi(s) \tag{4.93}$$

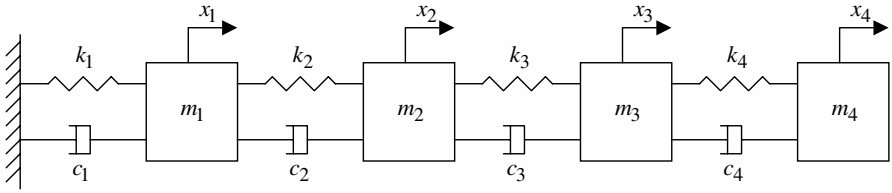

Figure 4.11: Mass-Stiffness-Damping System

Expanding the transfer function matrix in eqn. (4.93) as a power series yields

$$H[sI - F]^{-1}B = \frac{\phi_1}{s} + \frac{\phi_2}{s^2} + \frac{\phi_3}{s^3} + \cdots \tag{4.94}$$

where the continuous-time Markov parameters ϕ_i are given by

$$\phi_i = HF^{i-1}B \tag{4.95}$$

The continuous-time Markov parameters can be determined directly from the ERA. This is accomplished by first converting the discrete-time realization in eqn. (4.85) to a continuous-time realization using the methods described in §3.5. This continuous-time realization, denoted as $(\bar{F},\ \bar{B},\ \bar{H})$ may not necessarily be identical to the form in eqn. (4.92). However, both systems are similar, with

$$H[sI - F]^{-1}B = \bar{H}[sI - \bar{F}]^{-1}\bar{B} = \Phi(s) \tag{4.96a}$$

$$HF^{i-1}B = \bar{H}\bar{F}^{i-1}\bar{B} = \phi_i \tag{4.96b}$$

Therefore, there exists a similarity transformation T between the systems $(\bar{F},\ \bar{B},\ \bar{H})$ and $(F,\ B,\ H)$. This similarity transformation can be used to determine the mass, stiffness, and damping matrices. Yeh and Yang[27] showed that the similarity transformation is determined by

$$F = T\,\bar{F}\,T^{-1} \tag{4.97a}$$

$$B = T\,\bar{B} \tag{4.97b}$$

$$H = \bar{H}\,T^{-1} \tag{4.97c}$$

where

$$T = \begin{bmatrix} \bar{H} \\ \bar{H}\,\bar{F} \end{bmatrix} \tag{4.98}$$

The mass, stiffness, and damping matrices are obtained by

$$M = [\bar{H}\,\bar{F}\,\bar{B}]^{-1} \tag{4.99a}$$

$$\begin{bmatrix} K & C \end{bmatrix} = -M\,\bar{H}\,\bar{F}^2 T^{-1} \tag{4.99b}$$

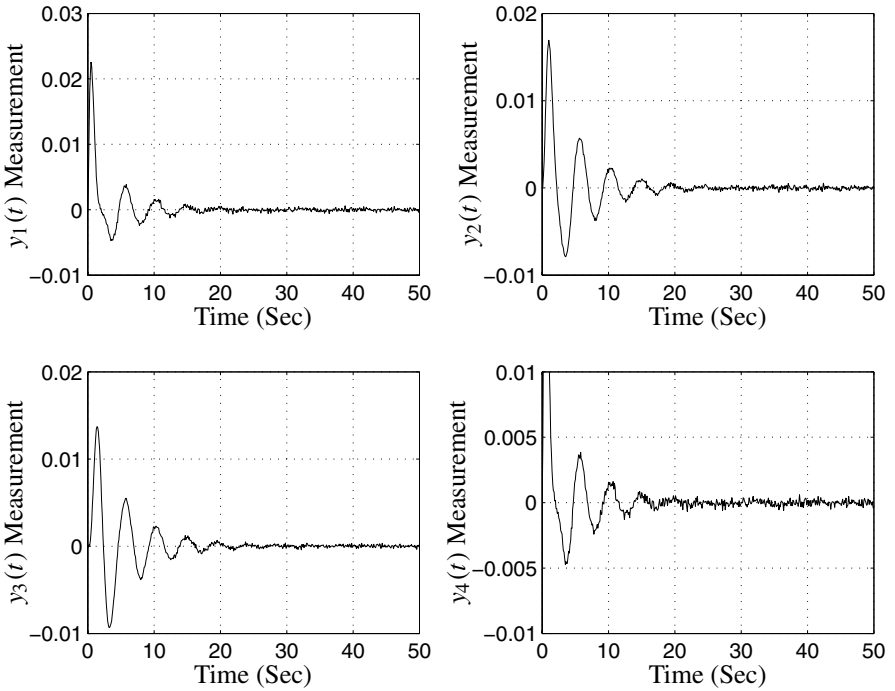

Figure 4.12: Simulated Position Measurements

Therefore, once a conversion of the ERA realized matrices from discrete-time to continuous-time is made, the modal properties and second-order matrix representations can be determined from eqn. (4.99). The ERA has been effectively used to determine system models for a wide variety of systems. More details on the ERA can be found in Ref. [28].

Example 4.5: In this example we will use the ERA to identify the mass, stiffness, and damping matrices of a 4 mode system from simulated mass-position measurements. This system is shown in Figure 4.11. The equations of motion can be found by using the techniques shown in §3.10. In this example the following mass-stiffness-damping matrices are used:

$$M = \begin{bmatrix} 1 & 0 & 0 & 0 \\ 0 & 1 & 0 & 0 \\ 0 & 0 & 1 & 0 \\ 0 & 0 & 0 & 1 \end{bmatrix}, \quad K = \begin{bmatrix} 10 & -5 & 0 & 0 \\ -5 & 10 & -5 & 0 \\ 0 & -5 & 10 & -5 \\ 0 & 0 & -5 & 10 \end{bmatrix}$$

$$C = \begin{bmatrix} 2 & -1 & 0 & 0 \\ -1 & 2 & -1 & 0 \\ 0 & -1 & 2 & -1 \\ 0 & 0 & -1 & 2 \end{bmatrix}$$

Note that proportional damping is given since $C = 1/5K$. In order to identify the system matrices using the ERA an impulse input is required at each mass, and the position of each mass must be measured. Therefore a total of 16 output measurements is required (4 position measurements for each impulse input). With the exact solution known, Gaussian white-noise of approximately 1% the size of the signal amplitude is added to simulate the output measurements. A 50-second simulation is performed, with measurements sampled every 0.1 seconds. A plot of the simulated position output measurements for an impulse input to the first mass is shown in Figure 4.12. Using all available measurements, the Hankel matrix in the ERA was chosen to be a 400×1600 dimension matrix. After computing the discrete-time state matrices using eqn. (4.85), a conversion to continuous-time state matrices is performed, and the mass, stiffness, and damping matrices are computed using eqn. (4.99). The results of this computation are

$$M = \begin{bmatrix} 1.0336 & -0.0144 & 0.0153 & -0.0071 \\ -0.0104 & 0.9857 & 0.0009 & -0.0013 \\ -0.0019 & 0.0208 & 0.9841 & 0.0060 \\ -0.0045 & 0.0067 & -0.0121 & 1.0166 \end{bmatrix}$$

$$K = \begin{bmatrix} 10.1728 & -5.1059 & 0.0709 & -0.0548 \\ -5.0897 & 9.9608 & -4.9498 & -0.0016 \\ 0.0281 & -4.9408 & 9.9469 & -5.0120 \\ -0.0656 & 0.0538 & -5.0408 & 10.0503 \end{bmatrix}$$

$$C = \begin{bmatrix} 1.9885 & -0.9877 & -0.0079 & 0.0004 \\ -0.9944 & 1.9855 & -0.9726 & -0.0222 \\ -0.0097 & -0.9461 & 1.9255 & -0.9612 \\ 0.0020 & -0.0073 & -1.0060 & 2.0195 \end{bmatrix}$$

These realized matrices are in close agreement to the true matrices. One drawback of the mass, stiffness, and damping identification method is that it does not produce matrices that are symmetric. A discussion on this issue is given in Ref. [29]. Obviously, the realized matrices are not physically consistent with the connectivity of Figure 4.11, and are simply a second-order representation of the system consistent with the measurements. Also, the true and identified natural frequencies and damping ratios are given below, which shows close agreement.

True		Identified	
ω_n	ζ	ω_n	ζ
1.3820	0.1382	1.3818	0.1381
2.6287	0.2629	2.6248	0.2622
3.6180	0.3618	3.5988	0.3686
4.2533	0.4253	4.2599	0.4129

4.6 Summary

In this chapter several applications of least squares methods have been presented for Global Positioning System navigation, spacecraft attitude determination from various sensor devices, orbit determination from ground-based sensors, aircraft parameter identification using on-board measurements, and modal identification of vibratory systems. These practical examples make extensive use of the tools derived in the previous chapters, and form the basis for "real-world" applications in dynamic systems. We anticipate that most readers, having gained computational and analytical experience from the examples of the first two chapters and elsewhere, will profit greatly by a careful study of these applications. The constraints imposed by the length of this text did not, however, permit an entirely self-contained and satisfactory development of the concepts introduced in the applications of this chapter. It will likely prove useful for the interested reader to pursue these important subjects in the cited literature.

A summary of the key formulas presented in this chapter is given below.

- GPS Pseudorange

$$\tilde{\rho}_i = [(s_{i1} - x)^2 + (s_{i2} - y)^2 + (s_{i3} - z)^2]^{1/2} + \tau + v_i, \ i = 1, 2, \ldots, n$$

- Vector Measurement Attitude Determination and Covariance

$$\mathbf{b} = A\mathbf{r}$$

$$J(\hat{A}) = \frac{1}{2}\sum_{j=1}^{N} \sigma_j^{-2} \|\tilde{\mathbf{b}}_j - \hat{A}\mathbf{r}_j\|^2, \quad \hat{A}\hat{A}^T = I_{3\times 3}$$

$$P = \left(-\sum_{j=1}^{N} \sigma_j^{-2} [A\,\mathbf{r}_j \times]^2 \right)^{-1}$$

- Davenport's Attitude Determination Algorithm

$$K \equiv -\sum_{j=1}^{N} \sigma_j^{-2} \Omega(\tilde{\mathbf{b}}_j) \Gamma(\mathbf{r}_j)$$

$$K\hat{\mathbf{q}} = \lambda \hat{\mathbf{q}}$$

- Orbit Determination

$$\ddot{\mathbf{r}} = -\frac{\mu}{||\mathbf{r}||^3}\mathbf{r}$$

$$\boldsymbol{\rho} = \mathbf{r} - \mathbf{R} = \begin{bmatrix} x - ||\mathbf{R}|| \cos\lambda \cos\theta \\ y - ||\mathbf{R}|| \cos\lambda \sin\theta \\ z - ||\mathbf{R}|| \sin\lambda \end{bmatrix}$$

$$\begin{bmatrix} \rho_u \\ \rho_e \\ \rho_n \end{bmatrix} = \begin{bmatrix} \cos\lambda & 0 & \sin\lambda \\ 0 & 1 & 0 \\ -\sin\lambda & 0 & \cos\lambda \end{bmatrix} \begin{bmatrix} \cos\theta & \sin\theta & 0 \\ -\sin\theta & \cos\theta & 0 \\ 0 & 0 & 1 \end{bmatrix} \boldsymbol{\rho}$$

$$||\boldsymbol{\rho}|| = (\rho_u^2 + \rho_e^2 + \rho_n^2)^{1/2}$$

$$\text{az} = \tan^{-1}\left(\frac{\rho_e}{\rho_n}\right)$$

$$\text{el} = \sin^{-1}\left(\frac{\rho_u}{||\boldsymbol{\rho}||}\right)$$

- Aircraft Parameter Identification

$$\dot{\mathbf{x}} = \mathbf{f}(t, \mathbf{x}, \mathbf{p})$$

$$\tilde{\mathbf{y}}_k = \mathbf{h}(t_k, \mathbf{x}_k) + \mathbf{v}_k$$

$$J(\hat{\mathbf{p}}) = \frac{1}{2} \sum_{k=1}^{N} (\tilde{\mathbf{y}}_k - \hat{\mathbf{y}}_k)^T R^{-1} (\tilde{\mathbf{y}}_k - \hat{\mathbf{y}}_k)$$

$$\hat{\mathbf{p}}_{i+1} = \hat{\mathbf{p}}_i - [\nabla^2_{\hat{\mathbf{p}}} J(\hat{\mathbf{p}})]^{-1} [\nabla_{\hat{\mathbf{p}}} J(\hat{\mathbf{p}})]$$

$$[\nabla_{\hat{\mathbf{p}}} J(\hat{\mathbf{p}})] = -\sum_{k=1}^{N} [\nabla_{\hat{\mathbf{p}}} \hat{\mathbf{y}}_k]^T R^{-1} (\tilde{\mathbf{y}}_k - \hat{\mathbf{y}}_k)$$

$$[\nabla^2_{\hat{\mathbf{p}}} J(\hat{\mathbf{p}})] \approx \sum_{k=1}^{N} [\nabla_{\hat{\mathbf{p}}} \hat{\mathbf{y}}_k]^T R^{-1} [\nabla_{\hat{\mathbf{p}}} \hat{\mathbf{y}}_k]$$

- Eigensystem Realization Algorithm

$$\mathbf{x}_{k+1} = \Phi \mathbf{x}_k + \Gamma \mathbf{u}_k$$

$$\mathbf{y}_k = H \mathbf{x}_k + D \mathbf{u}_k$$

$$Y_0 = D$$

$$Y_k = H \Phi^{k-1} \Gamma, \quad k > 1$$

$$\mathcal{H}_{k-1} = \begin{bmatrix} Y_k & Y_{k+m_1} & \cdots & Y_{k+m_{s-1}} \\ Y_{k+l_1} & Y_{k+l_1+m_1} & \cdots & Y_{k+l_1+m_{s-1}} \\ \vdots & \vdots & \ddots & \vdots \\ Y_{k+l_{r-1}} & Y_{k+l_{r-1}+m_1} & \cdots & Y_{k+l_{r-1}+m_{s-1}} \end{bmatrix}$$

$$\mathcal{H}_0 = P S Q^T$$

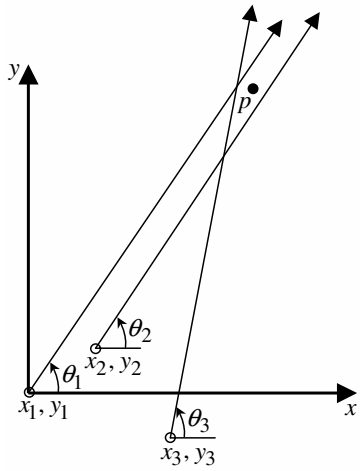

Figure 4.13: Planar Triangulation from Uncertain Base Points

$$\Phi = S^{-1/2} P^T \mathcal{H}_1 Q\, S^{-1/2}$$
$$\Gamma = S^{1/2} Q^T E_p$$
$$H = E_m^T P\, S^{1/2}$$
$$D = Y_0$$

Exercises

4.1 A problem closely related to the GPS position determination problem is planar triangulation. With reference to Figure 4.13, suppose a surveyor has collected data to estimate the location (x, y) of a point p. The point p is assumed, for simplicity, to lie in the $x - y$ plane. Suppose that the measurements consist of the azimuth θ of p from several imperfectly known points along a baseline (the x-axis). The first measurement base point is adopted as the origin $(x_1 = y_1 = 0)$ and the relative coordinates (x_2, y_2), (x_3, y_3) are admitted as four additional unknowns. The observations are modelled (refer to Figure 4.13) as

$$\tilde{\theta}_j = \tan^{-1}\left(\frac{y - y_j}{x - x_j}\right) + v_{\theta_j}, \quad j = 1, 2, 3$$
$$\tilde{x}_j = x_j + v_{x_j}, \quad j = 2, 3$$
$$\tilde{y}_j = y_j + v_{y_j}, \quad j = 2, 3$$

Thus, there are seven observed parameters $(\tilde{\theta}_1, \tilde{\theta}_2, \tilde{\theta}_3, \tilde{x}_2, \tilde{y}_2, \tilde{x}_3, \tilde{y}_3)$ and six unknown (to be estimated) parameters $(x, y, x_2, y_2, x_3, y_3)$. The dual role of (x_2, y_2, x_3, y_3) as observed and to-be-estimated parameters should present no particular conceptual difficulty if one recognizes that the measurement equations for these parameters are the simplest possible dependence of the observed parameters upon the unknown variables. The measurements and variances are given in the following table:

j	$\tilde{x}_j$	$\sigma^2_{x_j}$	$\tilde{y}_j$	$\sigma^2_{y_j}$	$\tilde{\theta}_j$	$\sigma^2_{\theta_j}$
1	0	0	0	0	30.1	0.01
2	500	100	50	144	45.0	0.01
3	1000	25	−100	100	73.6	0.01

Given the following starting estimates:

$$\begin{aligned}\mathbf{x}_c &= \begin{bmatrix} x_c & y_c & x_{2_c} & y_{2_c} & x_{3_c} & y_{3_c} \end{bmatrix}^T \\ &= \begin{bmatrix} 1210 & 700 & 500 & 50 & 1000 & -100 \end{bmatrix}^T\end{aligned}$$

and the measurements in the previous table, find estimates of the point p and base points using nonlinear least squares, and determine the associated covariance matrix. Also, program the Levenberg-Marquardt method of §1.6.3 and use this algorithm for improved convergence for various initial conditions.

4.2 Write a numerical algorithm based on the Levenberg-Marquardt method of §1.6.3 for the GPS navigation simulation in example 4.1. Can you achieve better convergence than nonlinear least squares for various starting conditions?

4.3 ♣ Consider the problem of determining the position and orientation of a vehicle using line-of-sight measurements from a vision-based beacon system based on Position Sensing Diode (PSD) technology,[30] depicted in Figure 4.14. If we choose the z-axis of the sensor coordinate system to be directed outward along the boresight of the PSD, then given object space (X, Y, Z) and image space (x, y, z) coordinate frames (see Figure 4.14), the ideal object to image space projective transformation (noiseless) can be written as follows:

$$x_i = -f\frac{A_{11}(X_i - X_c) + A_{12}(Y_i - Y_c) + A_{13}(Z_i - Z_c)}{A_{31}(X_i - X_c) + A_{32}(Y_i - Y_c) + A_{33}(Z_i - Z_c)}, \quad i = 1, 2, \ldots, N$$

$$y_i = -f\frac{A_{21}(X_i - X_c) + A_{22}(Y_i - Y_c) + A_{23}(Z_i - Z_c)}{A_{31}(X_i - X_c) + A_{32}(Y_i - Y_c) + A_{33}(Z_i - Z_c)}, \quad i = 1, 2, \ldots, N$$

where N is the total number of observations, (x_i, y_i) are the image space observations for the i^{th} line-of-sight, (X_i, Y_i, Z_i) are the known object space locations of the i^{th} beacon, (X_c, Y_c, Z_c) is the unknown object space location of the sensor, f is the known focal length, and A_{jk} are the unknown coefficients of the attitude matrix (A) associated to the orientation from the object plane to the image plane. The observation can be reconstructed in unit vector form as

$$\mathbf{b}_i = A\mathbf{r}_i, \quad i = 1, 2, \ldots, N$$

where

$$\mathbf{b}_i \equiv \frac{1}{\sqrt{f^2+x_i^2+y_i^2}}\begin{bmatrix}-x_i\\-y_i\\f\end{bmatrix}$$

$$\mathbf{r}_i \equiv \frac{1}{\sqrt{(X_i-X_c)^2+(Y_i-Y_c)^2+(Z_i-Z_c)^2}}\begin{bmatrix}X_i-X_c\\Y_i-Y_c\\Z_i-Z_c\end{bmatrix}$$

Write a nonlinear least squares program to determine the position and orientation from line-of-sight measurements. Assume the following six beacon locations:

$$\begin{aligned}
X_1 &= 0.5\text{m}, & Y_1 &= 0.5\text{m}, & Z_1 &= 0.0\text{m}\\
X_2 &= -0.5\text{m}, & Y_2 &= -0.5\text{m}, & Z_2 &= 0.0\text{m}\\
X_3 &= -0.5\text{m}, & Y_3 &= 0.5\text{m}, & Z_3 &= 0.0\text{m}\\
X_4 &= 0.5\text{m}, & Y_4 &= -0.5\text{m}, & Z_4 &= 0.0\text{m}\\
X_5 &= 0.2\text{m}, & Y_5 &= 0.0\text{m}, & Z_5 &= 0.1\text{m}\\
X_6 &= 0.0\text{m}, & Y_6 &= 0.2\text{m}, & Z_6 &= -0.1\text{m}
\end{aligned}$$

Any parameterization of the attitude matrix can be used, such as the Euler angles shown in §3.7.1; however, we suggest that the vector of modified Rodrigues parameters, $\mathbf{p}$, be used.[31] These parameters are closely related to the quaternions, with

$$\mathbf{p} = \frac{\boldsymbol{\varrho}}{1+q_4}$$

where the attitude matrix is given by

$$A(\mathbf{p}) = I_{3\times 3} - \frac{4(1-\mathbf{p}^T\mathbf{p})}{(1+\mathbf{p}^T\mathbf{p})^2}[\mathbf{p}\times] + \frac{8}{(1+\mathbf{p}^T\mathbf{p})^2}[\mathbf{p}\times]^2$$

To help you along it can be shown that the partial of $A(\mathbf{p})\mathbf{r}$ with respect to $\mathbf{p}$ is given by[32]

$$\frac{\partial A(\mathbf{p})\mathbf{r}}{\partial \mathbf{p}} = \frac{4}{(1+\mathbf{p}^T\mathbf{p})^2}[A(\mathbf{p})\mathbf{r}\times]\left\{(1-\mathbf{p}^T\mathbf{p})I_{3\times 3} - 2[\mathbf{p}\times] + 2\mathbf{p}\mathbf{p}^T\right\}$$

Consider a $1,800$-second simulation (i.e., $t_f = 1800$), and a focal length of $f = 1$. The true vehicle linear motion is given by $X_c = 30\exp[-(1/300)t]$ m, $Y_c = 30-(30/1800)t$ m, and $Z_c = 10-(10/1800)t$ m. The true angular motion is given by $\omega_1 = 0$ rad/sec, $\omega_2 = -0.0011$ rad/sec, and $\omega_3 = 0$ rad/sec, with zero initial conditions for the orientation angles. The measurement error is assumed to be zero-mean Gaussian with a standard deviation of $1/5000$ of the focal plane dimension, which for a 90 degree field-of-view corresponds to an angular resolution of $90/5000 \simeq 0.02$ degrees. For simplicity assume a measurement model given by $\tilde{\mathbf{b}} = A\mathbf{r} + \mathbf{v}$, where the covariance of $\mathbf{v}$ is assumed to be a diagonal matrix with elements given by $0.02\pi/180$. Find position and orientation estimates for this maneuver at 0.01-second intervals using the nonlinear least squares program, and determine the associated error-covariance matrix.

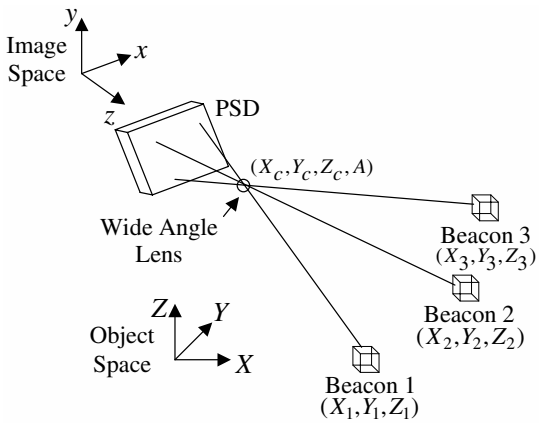

Figure 4.14: Vision Navigation System

4.4 Instead of determining the position of the PSD sensor shown in exercise 4.3, suppose we wish to determine a fixed attitude matrix, A, and focal length, f, given known positions X_c, Y_c, and Z_c over time. Develop a nonlinear least squares program to perform this calibration task using the true position location trajectories (X_c, Y_c, Z_c) shown in exercise 4.3. First, try determining the focal length only using some known fixed attitude. Then, try estimating both the fixed attitude matrix and focal length. How sensitive is your algorithm to initial guesses? Try various other known position motions to test the convergence properties of your algorithm. Also, try implementing the Levenberg-Marquardt algorithm of §1.6.3 to provide a more robust algorithm.

4.5 Given two non-parallel reference unit vectors $\mathbf{r}_1$ and $\mathbf{r}_2$ and the corresponding observation unit vectors $\mathbf{b}_1$ and $\mathbf{b}_2$, the TRIAD algorithm finds an orthogonal attitude matrix A that satisfies (in the noiseless case)

$$\mathbf{b}_1 = A\mathbf{r}_1, \quad \mathbf{b}_2 = A\mathbf{r}_2$$

This algorithm is given by first constructing two triads of manifestly orthonormal reference and observation vectors:

$$\mathbf{u}_1 = \mathbf{r}_1, \quad \mathbf{u}_2 = (\mathbf{r}_1 \times \mathbf{r}_2)/||(\mathbf{r}_1 \times \mathbf{r}_2)||$$
$$\mathbf{u}_3 = [\mathbf{r}_1 \times (\mathbf{r}_1 \times \mathbf{r}_2)]/||(\mathbf{r}_1 \times \mathbf{r}_2)||$$

$$\mathbf{v}_1 = \mathbf{b}_1, \quad \mathbf{v}_2 = (\mathbf{b}_1 \times \mathbf{b}_2)/||(\mathbf{b}_1 \times \mathbf{b}_2)||$$
$$\mathbf{v}_3 = [\mathbf{b}_1 \times (\mathbf{b}_1 \times \mathbf{b}_2)]/||(\mathbf{b}_1 \times \mathbf{b}_2)||$$

and then forming the following orthogonal matrices:

$$U = \begin{bmatrix}\mathbf{u}_1 & \mathbf{u}_2 & \mathbf{u}_3\end{bmatrix}, \quad V = \begin{bmatrix}\mathbf{v}_1 & \mathbf{v}_2 & \mathbf{v}_3\end{bmatrix}$$

Prove that U and V are orthogonal. Next, prove that the attitude matrix A is given by $A = V U^T$.

4.6 Using eqns. (4.15) to (4.17), prove that the attitude error covariance is given by the expression in eqn. (4.18).

4.7 ♣ Prove that the matrix K in eqn. (4.24) is also given by

$$K = \begin{bmatrix} S - \alpha I & \mathbf{z} \\ \mathbf{z}^T & \alpha \end{bmatrix}$$

where

$$B = \sum_{j=1}^{N} \sigma_j^{-2} \tilde{\mathbf{b}}_j \mathbf{r}_j^T$$

$$\alpha = \mathrm{Tr} B = \sum_{j=1}^{N} \sigma_j^{-2} \tilde{\mathbf{b}}_j^T \mathbf{r}_j$$

$$S = B + B^T = \sum_{j=1}^{N} \sigma_j^{-2} (\tilde{\mathbf{b}}_j \mathbf{r}_j^T + \mathbf{r}_j \tilde{\mathbf{b}}_j^T)$$

$$\mathbf{z} = \sum_{j=1}^{N} \sigma_j^{-2} (\tilde{\mathbf{b}}_j \times \mathbf{r}_j)$$

4.8 Write a computer program to determine the optimal attitude from vector observations given by algorithms from Davenport in eqn. (4.26). Assuming a Gaussian distribution of stars, create a random sample of stars on a uniform sphere (note: the actual star distribution more closely follows a Poisson distribution[33]). Randomly pick 2 to 6 stars within an 8 degree field-of-view to simulate a star camera. Then, create synthetic body measurements with the measurement error for the camera given in example 4.2. Assuming a true attitude motion given by a constant angular velocity about the y-axis with $\boldsymbol{\omega} = \begin{bmatrix} 0 & -0.0011 & 0 \end{bmatrix}^T$ rad /sec. Compute an attitude solution every second using both methods. Using the covariance expression in eqn. (4.18), numerically show that the 3σ bounds do indeed bound the attitude errors.

4.9 ♣ A problem that is closely related to the attitude determination problem involves determining ellipse parameters from measured data. Figure 4.15 depicts a general ellipse rotated by an angle θ. The basic equation of an ellipse is given by

$$\frac{(x' - x_0')^2}{a^2} + \frac{(y' - y_0')^2}{b^2} = 1$$

where (x_0', y_0') denotes the origin of the ellipse and (a, b) are positive values. The coordinate transformation follows

$$x' = x \cos\theta + y \sin\theta$$
$$y' = -x \sin\theta + y \cos\theta$$

Show that the ellipse equation can be rewritten as

$$Ax^2 + Bxy + Cy^2 + Dx + Ey + F = 0$$

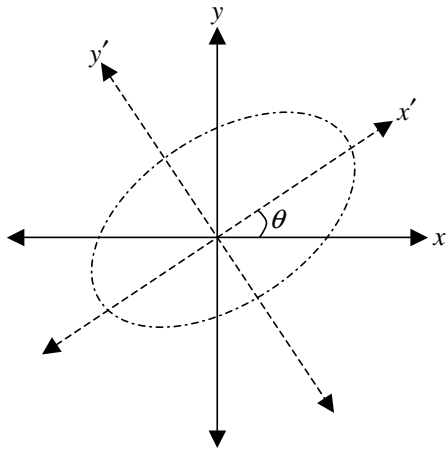

Figure 4.15: Ellipse with Rotation

Next, determine a form for the set of the coefficients so that the following constraint is always satisfied: $A^2 + 0.5B^2 + C^2 = 1$.[34]

Given a set of coefficients A, B, C, D, E, and F, show that the formulas for θ, a, b, x_0', and y_0' are given by

$$\cot(2\theta) = \frac{A - C}{B}$$

$$a = \sqrt{\frac{Q'}{A'}}, \quad b = \sqrt{\frac{Q'}{C'}}$$

$$x_0' = -\frac{D'}{2A'}, \quad y_0' = -\frac{E'}{2C'}$$

where

$$A' = A\cos^2\theta + B\sin\theta\cos\theta + C\sin^2\theta$$

$$B' = B(\cos^2\theta - \sin^2\theta) + 2(C - A)\sin\theta\cos\theta = 0$$

$$C' = A\sin^2\theta - B\sin\theta\cos\theta + C\cos^2\theta$$

$$D' = D\cos\theta + E\sin\theta$$

$$E' = -D\sin\theta + E\cos\theta$$

$$F' = F$$

$$Q' \equiv A'\left(\frac{D'}{2A'}\right)^2 + C'\left(\frac{E'}{2C'}\right)^2 - F'$$

(hint: show that the new variables follow the rotated ellipse equation: $A'x'^2 + B'x'y' + C'y'^2 + D'x' + E'y' + F' = 0$).

Suppose that a set of measurements for x and y exist, and we form the following vector of unknown parameters: $\mathbf{x} \equiv \begin{bmatrix} A & B & C & D & E & F \end{bmatrix}^T$. Our goal is

to determine an estimate of $\mathbf{x}$ from this measured data set. Show that the minimum norm loss function can be written as

$$J(\hat{\mathbf{x}}) = \hat{\mathbf{x}}^T H^T H \hat{\mathbf{x}}$$

subject to

$$\hat{\mathbf{x}}^T Z \hat{\mathbf{x}} = 1$$

where the i^{th} row of H is given by

$$H_i = \begin{bmatrix} \tilde{x}_i^2 & \tilde{x}_i \tilde{y}_i & \tilde{y}_i^2 & \tilde{x}_i & \tilde{y}_i & 1 \end{bmatrix}$$

Determine the matrix Z that satisfies the constraint. Using the eigenvalue method of §4.2 find the form for the optimal solution for $\hat{\mathbf{x}}$. Write a computer program for your derived solution and perform a simulation to test your algorithm. Note, a more robust approach involves using a reduced eigenvalue decomposition[35] or a singular value decomposition approach.[36]

4.10 A simple solution to the ellipse parameter identification system shown in exercise 4.9 involves using least squares. The ellipse parameter formulas shown in this problem are invariant under scalar multiplication (i.e., if we multiply A, B, C, etc., by a scalar then the formulas to determine θ, a, b, x_0', and y_0' remain unchanged). Therefore, we can assume that $F = 1$ without loss in generality. Derive an unconstrained least squares solution that estimates A, B, C, D, and E with the "measurement" given by $F = 1$. Test your algorithm using different simulation scenarios.

4.11 ♣ Consider the ellipse identification system shown in exercise 4.9. Using any estimation algorithm a set of reconstructed variables for x and y can be given by using the estimates of the coefficients A, B, C, D, E, and F. Suppose that $\hat{x}$ and $\hat{y}$ denote these estimated values, and $\tilde{x}$ and $\tilde{y}$ denote the measurement values. The current problem involves a method to check the consistency of the residuals between the measured and estimated x and y values. First, show that the measured data must satisfy the following inequalities in order for the data to conform to the ellipse model:

$$(B\tilde{x} + E)^2 - 4C(A\tilde{x}^2 + D\tilde{x} + F) > 0$$
$$(B\tilde{y} + D)^2 - 4A(C\tilde{y}^2 + E\tilde{y} + F) > 0$$

Suppose that the residual is defined as

$$f(\tilde{x}, \tilde{y}) \equiv A\tilde{x}^2 + B\tilde{x}\tilde{y} + C\tilde{y}^2 + D\tilde{x} + E\tilde{y} + F$$

Ideally $f(\tilde{x}, \tilde{y})$ should be zero, but this does not occur in practice due to measurement noise. Show that linearizing $f(\tilde{x}, \tilde{y})$ about $\hat{x}$ and $\hat{y}$ leads to

$$f(\tilde{x}, \tilde{y}) - f(\hat{x}, \hat{y}) = (2A\hat{x} + B\hat{y} + D)(\tilde{x} - \hat{x}) + (2C\hat{y} + B\hat{x} + E)(\tilde{y} - \hat{y})$$

Using this equation derive an expression for the variance of residual. Finally, using this expression derive a consistency test to remove extraneous measurement points (i.e., points outside some defined σ bound). Test your algorithm using simulated data points.

4.12 From the analysis of §4.2.4, show that the expressions for each of the eigenvalues in eqns. (4.31) and (4.33), and eigenvectors in eqns. (4.35), (4.37), and (4.40), do indeed satisfy $\lambda \mathbf{v} = F\mathbf{v}$.

4.13 Show that the expressions for the eigenvalues in eqn. (4.41), and eigenvectors in eqn. (4.42), reduce down from the eigenvalues in eqns. (4.31) and (4.33), and eigenvectors, in eqns. (4.35), (4.37), and (4.40), under the assumptions that $\mathbf{b}_1$ and $\mathbf{b}_2$ are unit vectors and $\sigma_1^2 = \sigma_2^2 \equiv \sigma^2$. Furthermore, prove that the vectors in eqn. (4.42) form an orthonormal set.

4.14 An alternative to using vector measurements to determine the attitude of a vehicle involves using GPS phase difference measurements.[37] The measurement model using GPS measurements is given by

$$\Delta\tilde{\phi}_{ij} = \mathbf{b}_i^T A \mathbf{s}_j + v_{ij}$$

where $\mathbf{s}_j$ is the known line-of-sight to the GPS spacecraft in reference-frame coordinates, $\mathbf{b}_i$ is the baseline vector between two antennae in body-frame coordinates, $\Delta\tilde{\phi}_{ij}$ denotes the phase difference measurement for the i^{th} baseline and j^{th} sightline, and v_{ij} represents a zero-mean Gaussian measurement error with standard deviation σ_{ij} which is $0.5\text{cm}/\lambda = 0.026$ wavelengths for typical phase noise.[37] At each epoch it is assumed that m baselines and n sightlines exist.

Attitude determination using GPS signals involves finding the proper orthogonal matrix $\hat{A}$ that minimizes the following generalized loss function:

$$J(\hat{A}) = \frac{1}{2}\sum_{i=1}^{m}\sum_{j=1}^{n}\sigma_{ij}^{-2}(\Delta\tilde{\phi}_{ij} - \mathbf{b}_i^T \hat{A}\mathbf{s}_j)^2$$

Substitute eqn. (4.17) into this loss function, and after taking the appropriate partials show that the following optimal error covariance can be derived:

$$P = \left(\sum_{i=1}^{m}\sum_{j=1}^{n}\sigma_{ij}^{-2}[A\mathbf{s}_j\times]\mathbf{b}_i\,\mathbf{b}_i^T[A\mathbf{s}_j\times]^T\right)^{-1}$$

Note that the optimal covariance requires knowledge of the attitude matrix.

4.15 Consider the problem of converting the GPS attitude determination problem into a form given by Wahba's problem.[38] This is accomplished by converting the sightline vectors into the body frame, denoted by $\overline{\mathbf{s}}_j$. Assuming that at least three non-coplanar baselines exist, this conversion is given by

$$\overline{\mathbf{s}}_j = M_j^{-1}\mathbf{y}_j$$

where

$$M_j = \sum_{i=1}^{m}\sigma_{ij}^{-2}\mathbf{b}_i\,\mathbf{b}_i^T \quad \text{for } j = 1, 2, \ldots, n$$

$$\mathbf{y}_j = \sum_{i=1}^{m}\sigma_{ij}^{-2}\Delta\tilde{\phi}_{ij}\mathbf{b}_i \quad \text{for } j = 1, 2, \ldots, n$$

Then, given multiple (converted) body and known reference sightline vectors, Davenport's method of §4.2.3 can be employed to determine the attitude. It can be shown that this approach is suboptimal though. The covariance of this suboptimal approach is given by

$$P_s = \left(\sum_{j=1}^{n} a_j [\bar{\mathbf{s}}_j \times]^2\right)^{-1} \left(\sum_{j=1}^{n} a_j^2 [\bar{\mathbf{s}}_j \times] P_j [\bar{\mathbf{s}}_j \times]^T\right) \left(\sum_{j=1}^{n} a_j [\bar{\mathbf{s}}_j \times]^2\right)^{-1} \tag{4.100}$$

From the Cramér-Rao inequality we know that $P_s \geq P$, where P is given in exercise 4.14. Under what conditions does $P_s = P$? Prove your answer.

4.16 In this exercise you will simulate the performance of the conversion of the GPS attitude determination problem into a form given by Wahba's problem, discussed in exercise 4.15. Simulate the motion of a spacecraft as given in exercise 4.8. Assume that the spacecraft is always in the view of two GPS satellites with constant sightlines given by

$$\mathbf{s}_1 = (1/\sqrt{3})\begin{bmatrix}1 & 1 & 1\end{bmatrix}^T, \quad \mathbf{s}_2 = (1/\sqrt{2})\begin{bmatrix}0 & 1 & 1\end{bmatrix}^T$$

The three normalized baseline cases are given by the following:
Case 1:

$$\mathbf{b}_1 = (1/\sqrt{1.09})\begin{bmatrix}1 & 0.3 & 0\end{bmatrix}^T, \quad \mathbf{b}_2 = \begin{bmatrix}0 & 1 & 0\end{bmatrix}^T$$
$$\mathbf{b}_3 = \begin{bmatrix}0 & 0 & 1\end{bmatrix}^T$$

Case 2:

$$\mathbf{b}_1 = (1/\sqrt{2})\begin{bmatrix}1 & 1 & 0\end{bmatrix}^T, \quad \mathbf{b}_2 = \begin{bmatrix}0 & 1 & 0\end{bmatrix}^T$$
$$\mathbf{b}_3 = \begin{bmatrix}0 & 0 & 1\end{bmatrix}^T$$

Case 3:

$$\mathbf{b}_1 = (1/\sqrt{1.02})\begin{bmatrix}0.1 & 1 & 0.1\end{bmatrix}^T, \quad \mathbf{b}_2 = \begin{bmatrix}0 & 1 & 0\end{bmatrix}^T$$
$$\mathbf{b}_3 = \begin{bmatrix}0 & 0 & 1\end{bmatrix}^T$$

The noise for each phase difference measurement is assumed to have a normalized standard deviation of $\sigma = 0.001$. To quantify the error introduced by the conversion to Wahba's form, use the following error factor:

$$f = \frac{1}{m_{\text{tot}}} \sum_{k=1}^{m_{\text{tot}}} \frac{\text{Tr}\left\{\text{diag}\left[P_s(t_k)^{1/2}\right]\right\}}{\text{Tr}\left\{\text{diag}\left[P(t_k)^{1/2}\right]\right\}}$$

where m_{tot} is the total number of measurements, P is given in exercise 4.14, and P_s is given in exercise 4.15. Compute the error factor f for each case. Also, show the 3σ bounds from P and P_s for each case. Which case produces the greatest errors?

4.17 Consider the problem of determining the state (position, $\mathbf{r}$, and velocity, $\dot{\mathbf{r}}$) and drag parameter of a vehicle at launch. The drag vector on the vehicle, which is modelled as a particle, is defined by

$$\mathbf{D} = -\left(\frac{1}{2}\rho V^2\right) C_D A \left(\frac{\dot{\mathbf{r}}}{V}\right)$$

where ρ is the density, $V \equiv ||\dot{\mathbf{r}}||$, C_D is the drag coefficient, and A is the projected area. This equation can be rewritten as

$$\mathbf{D} = -p\, m\, V\, \dot{\mathbf{r}}$$

where m is the mass of the vehicle and p is the drag parameter, given by

$$p \equiv \left(\frac{1}{2}\rho V^2\right) C_D A$$

Range and angle observations are assumed:

$$r = \sqrt{x^2 + y^2 + z^2}$$
$$\phi = \tan^{-1}\left(\frac{y}{x}\right)$$
$$\theta = \sin^{-1}\left(\frac{z}{r}\right)$$

with $\mathbf{r} = \begin{bmatrix} x & y & z \end{bmatrix}^T$. The equations of motion are given by

$$\ddot{x} = -p\,\dot{x}\,V$$
$$\ddot{y} = -p\,\dot{y}\,V$$
$$\ddot{z} = -g - p\,\dot{z}\,V$$

where $g = 9.81\ \mathrm{m/s^2}$. Create synthetic measurements sampled at 0.1-second intervals over a 20-second simulation by numerically integrating the equations of motion. Use a standard deviation of 10 m for the range measurement errors, and 0.01 rad for both angle measurement errors. Assume initial conditions of $\{x_0,\ y_0,\ z_0\} = \{-1000,\ -2000,\ 500\}$ m and $\{\dot{x}_0,\ \dot{y}_0,\ \dot{z}_0\} = \{100,\ 150,\ 50\}$ m/s. Also, set the drag parameter to

$$p = \frac{0.01}{\sqrt{\dot{x}_0^2 + \dot{y}_0^2 + \dot{z}_0^2}}$$

Using the nonlinear least-square differential correction algorithm depicted in Figure 4.8, estimate the initial conditions for position and velocity as well as the drag parameter (derive an analytical solution for the state transition matrix).

4.18 From eqns. (4.55) and (4.56) prove the following identity:

$$u_3^2 = \frac{1}{6}\chi^3 u_3 + u_5(u_1 - \chi)$$

4.19 ♣ Derive the Herrick-Gibbs formula in eqn. (4.66) by using the following Taylor series expansion:

$$\mathbf{r}_1 - \mathbf{r}_2 \approx -\tau_{12}\frac{d\mathbf{r}_2}{dt} + \frac{1}{2}\tau_{12}^2\frac{d^2\mathbf{r}_2}{dt^2} + \frac{1}{6}\tau_{12}^3\frac{d^3\mathbf{r}_2}{dt^3} + \frac{1}{24}\tau_{12}^4\frac{d^4\mathbf{r}_2}{dt^4}$$

$$\mathbf{r}_3 - \mathbf{r}_2 \approx -\tau_{23}\frac{d\mathbf{r}_2}{dt} + \frac{1}{2}\tau_{23}^2\frac{d^2\mathbf{r}_2}{dt^2} + \frac{1}{6}\tau_{23}^3\frac{d^3\mathbf{r}_2}{dt^3} + \frac{1}{24}\tau_{23}^4\frac{d^4\mathbf{r}_2}{dt^4}$$

Note, expressions for $\ddot{\mathbf{r}}_1$, $\ddot{\mathbf{r}}_2$, and $\ddot{\mathbf{r}}_3$ can be eliminated by using the inverse square law in eqn. (3.198).

4.20 Given the weakly coupled nonlinear oscillators

$$\ddot{x} = -\omega_1^2 x + \epsilon x z + A\cos\Omega_1 t$$

$$\ddot{z} = -\omega_1^2 z + \epsilon x z + B\cos\Omega_2 t$$

and the measurement model equation

$$\tilde{y}(t) = Cx + Dz + v \tag{4.101}$$

where ω_1^2, ω_2^2, Ω_1, Ω_2, A, B, C, D, and ϵ are constants, and $E\{v\} = 0$, $E\{v^2(t_j)\} = r$, and $E\{v(t_i)v(t_j)\} = 0$. Consider the following estimation problems:

(A) The model parameters $(\omega_1^2, \omega_2^2, \Omega_1, \Omega_2, A, B, C, D, \epsilon)$ are given constants, $\tilde{y}$ can be measured at m discrete instants; it is desired to estimate the initial state vector $\mathbf{x}(t_0) = \left[x(t_0)\ z(t_0)\ \dot{x}(t_0)\ \dot{z}(t_0)\right]^T$, given an initial estimate $\hat{\mathbf{x}}_a(t_0)$ and associated covariance matrix $P(t_0)$.

(B) The nine model parameters are uncertain, $\tilde{y}$ can be measured at m discrete instants, it is desired to estimate the initial state vector $\mathbf{x}(t_0)$ and the nine model parameters $(\omega_1^2, \omega_2^2, \Omega_1, \Omega_2, A, B, C, D, \epsilon)$, given *a priori* estimates and an associated covariance matrix.

Using the methods of the previous chapters, formulate minimal variance estimation algorithms for the aforementioned problems. Implement these algorithms as computer programs and study the performance of the algorithms (use synthetic measured data generated by adding zero-mean Gaussian distributed random numbers to perfect calculated y-values, see how well the true initial state and model parameter values are recovered).

4.21 Write a computer program to reproduce the orbit determination results in example 4.3. Also, write a numerical algorithm that replaces the nonlinear least squares iterations with the Levenberg-Marquardt method of §1.6.3. Can you achieve better results using this method over nonlinear least squares for poor initial guesses?

4.22 Consider the following nonlinear equations of motion for a highly maneuverable aircraft:

$$\dot{\alpha} = \dot{\theta} - \alpha^2\dot{\theta} - 0.09\alpha\dot{\theta} - 0.88\alpha + 0.47\alpha^2 + 3.85\alpha^3$$
$$- 0.22\delta_E + 0.28\delta_E\alpha^2 + 0.47\delta_E^2\alpha + 0.63\delta_E^3 - 0.02\theta^2$$

$$\ddot{\theta} = -0.396\dot{\theta} - 4.208\alpha - 0.470\alpha^2 - 3.564\alpha^3$$
$$- 20.967\delta_E + 6.265\delta_E\alpha^2 + 46.00\delta_E^2 + 61.40\delta_E^3$$

Using a known "rich" input for δ_E create synthetic measurements of the angle of attack α and pitch angle θ with zero initial conditions. Assume standard deviations of the measurement errors to be the same as the ones given in exercise 4.4. Then use the results of §4.4 to identify various parameters of the above model. Which parameters can be most accurately identified?

4.23 Write a computer program to reproduce the aircraft parameter identification results in example 4.4. Compare the performance of the algorithm using the second gradient in eqn. (4.70b) and its approximation in eqn. (4.71). Also, expand upon the computer program for parameter identification of the lateral parameters of the simulated 747 aircraft (described in exercise 3.30). Finally, write a program that couples the longitudinal and lateral identification process.

4.24 Prove the similarity transformation for the identification of the mass, stiffness, and damping matrices in eqn. (4.99).

4.25 Write a general computer program for the Eigensystem Realization Algorithm, and the mass, stiffness, and damping matrix identification approach using eqn. (4.99). Use the computer program to reproduce the results in example 4.5.

References

[1] Axelrad, P. and Brown, R.G., "GPS Navigation Algorithms," *Global Positioning System: Theory and Applications*, edited by B. Parkinson and J. Spilker, Vol. 64 of *Progress in Astronautics and Aeronautics*, chap. 9, American Institute of Aeronautics and Astronautics, Washington, DC, 1996.

[2] Parkinson, B.W., "GPS Error Analysis," *Global Positioning System: Theory and Applications*, edited by B. Parkinson and J. Spilker, Vol. 64 of *Progress in Astronautics and Aeronautics*, chap. 11, American Institute of Aeronautics and Astronautics, Washington, DC, 1996.

[3] Bate, R.R., Mueller, D.D., and White, J.E., *Fundamentals of Astrodynamics*, Dover Publications, New York, NY, 1971.

[4] Slater, M.A., Miller, A.C., Warren, W.H., and Tracewell, D.A., "The New SKYMAP Master Catalog (Version 4.0)," *Advances in the Astronautical Sciences*, Vol. 90, Aug. 1995, pp. 67–81.

[5] Light, D.L., "Satellite Photogrammetry," *Manual of Photogrammetry*, edited by C.C. Slama, chap. 17, American Society of Photogrammetry, Falls Church, VA, 4th ed., 1980.

[6] Mortari, D., "Search-Less Algorithm for Star Pattern Recognition," *Journal of the Astronautical Sciences*, Vol. 45, No. 2, April-June 1997, pp. 179–194.

[7] Shuster, M.D., "Maximum Likelihood Estimation of Spacecraft Attitude," *The Journal of the Astronautical Sciences*, Vol. 37, No. 1, Jan.-March 1989, pp. 79–88.

[8] Wahba, G., "A Least-Squares Estimate of Satellite Attitude," *SIAM Review*, Vol. 7, No. 3, July 1965, pp. 409.

[9] Lerner, G.M., "Three-Axis Attitude Determination," *Spacecraft Attitude Determination and Control*, edited by J.R. Wertz, chap. 12, Kluwer Academic Publishers, The Netherlands, 1978.

[10] Shuster, M.D., "Attitude Determination from Vector Observations," *Journal of Guidance and Control*, Vol. 4, No. 1, Jan.-Feb. 1981, pp. 70–77.

[11] Mortari, D., "ESOQ: A Closed-Form Solution of the Wahba Problem," *Journal of the Astronautical Sciences*, Vol. 45, No. 2, April-June 1997, pp. 195–204.

[12] Markley, F.L., "Attitude Determination Using Vector Observations and the Singular Value Decomposition," *The Journal of the Astronautical Sciences*, Vol. 36, No. 3, July-Sept. 1988, pp. 245–258.

[13] Sun, D. and Crassidis, J.L., "Observability Analysis of Six-Degree-of-Freedom Configuration Determination Using Vector Observations," *Journal of Guidance, Control, and Dynamics*, Vol. 25, No. 6, Nov.-Dec. 2002, pp. 1149–1157.

[14] Battin, R.H., *An Introduction to the Mathematics and Methods of Astrodynamics*, American Institute of Aeronautics and Astronautics, Inc., New York, NY, 1987.

[15] Escobal, P.E., *Methods of Orbit Determination*, Krieger Publishing Company, Malabar, FL, 1965.

[16] Vallado, D.A. and McClain, W.D., *Fundamentals of Astrodynamics and Applications*, McGraw-Hill, New York, NY, 1997.

[17] Yunck, T.P., "Orbit Determination," *Global Positioning System: Theory and Applications*, edited by B. Parkinson and J. Spilker, Vol. 164 of *Progress in Astronautics and Aeronautics*, chap. 21, American Institute of Aeronautics and Astronautics, Washington, DC, 1996.

[18] Iliff, K.W., "Parameter Estimation of Flight Vehicles," *Journal of Guidance, Control, and Dynamics*, Vol. 12, No. 5, Sept.-Oct. 1989, pp. 261–280.

[19] Roskam, J., *Airplane Flight Dynamics and Automatic Flight Controls*, Design, Analysis and Research Corporation, Lawrence, KS, 1994.

[20] Aström, K.J. and Eykhoff, P., "System Identification-A Survey," *Automatica*, Vol. 7, No. 2, March 1971, pp. 123–162.

[21] Franklin, G.F., Powell, J.D., and Workman, M., *Digital Control of Dynamic Systems*, Addison Wesley Longman, Menlo Park, CA, 3rd ed., 1998.

[22] Yeh, F.B. and Yang, C.D., "New Time-Domain Identification Technique," *Journal of Guidance, Control, and Dynamics*, Vol. 10, No. 3, May-June 1987, pp. 313–316.

[23] Ibrahim, S.R. and Mikulcik, E.C., "A New Method for the Direct Identification of Vibration Parameters from the Free Response," *Shock and Vibration Bulletin*, Vol. 47, No. 4, Sept. 1977, pp. 183–198.

[24] Juang, J.N. and Pappa, R.S., "An Eigensystem Realization Algorithm for Modal Parameter Identification and Model Reduction," *Journal of Guidance, Control, and Dynamics*, Vol. 8, No. 5, Sept.-Oct. 1985, pp. 620–627.

[25] Juang, J.N., Phan, M., Horta, L.G., and Longman, R.W., "Identification of Observer/Kalman Filer Markov Parameters: Theory and Experiments," *Journal of Guidance, Control, and Dynamics*, Vol. 16, No. 2, March-April 1993, pp. 320–329.

[26] Juang, J.N. and Pappa, R.S., "Effects of Noise on Modal Parameters Identified by the Eigensystem Realization Algorithm," *Journal of Guidance, Control, and Dynamics*, Vol. 9, No. 3, May-June 1986, pp. 294–303.

[27] Yang, C.D. and Yeh, F.B., "Identification, Reduction, and Refinement of Model Parameters by the Eigensystem Realization Algorithm," *Journal of Guidance, Control, and Dynamics*, Vol. 13, No. 6, Nov.-Dec. 1990, pp. 1051–1059.

[28] Juang, J.N., *Applied System Identification*, Prentice Hall, Englewood Cliffs, NJ, 1994.

[29] Rajaram, S. and Junkins, J.L., "Identification of Vibrating Flexible Structures," *Journal of Guidance, Control, and Dynamics*, Vol. 8, No. 4, July-Aug. 1985, pp. 463–470.

[30] Junkins, J.L., Hughes, D.C., Wazni, K.P., and Pariyapong, V., "Vision-Based Navigation for Rendezvous, Docking and Proximity Operations," *22nd Annual AAS Guidance and Control Conference*, Breckenridge, CO, Feb. 1999, AAS 99-021.

[31] Shuster, M.D., "A Survey of Attitude Representations," *Journal of the Astronautical Sciences*, Vol. 41, No. 4, Oct.-Dec. 1993, pp. 439–517.

[32] Crassidis, J.L. and Markley, F.L., "Attitude Estimation Using Modified Rodrigues Parameters," *Proceedings of the Flight Mechanics/Estimation Theory*

Symposium, NASA-Goddard Space Flight Center, Greenbelt, MD, May 1996, pp. 71–83.

[33] Markley, F.L., Bauer, F.H., Deily, J.J., and Femiano, M.D., "Attitude Control System Conceptual Design for Geostationary Operational Environmental Satellite Spacecraft Series," *Journal of Guidance, Control, and Dynamics*, Vol. 18, No. 2, March-April 1995, pp. 247–255.

[34] Bookstein, F.L., "Fitting Conic Sections to Scattered Data," *Computer Graphics and Image Processing*, Vol. 9, 1979, pp. 56–71.

[35] Halíř, R. and Flusser, J., "Numerically Stable Direct Least Squares Fitting of Ellipses," *6th International Conference in Central Europe on Computer Graphics and Visualization, WSCG '98*, University of West Bohemia, Campus Bory, Plzen - Bory, Czech Republic, Feb. 1998, pp. 125–132.

[36] Gander, W., Golub, G.H., and Strebel, R., "Least-Squares Fitting of Circles and Ellipses," *Numerical analysis (in honour of Jean Meinguet)*, edited by editorial board Bulletin Belgian Mathematical Society, 1996, pp. 63–84.

[37] Cohen, C.E., "Attitude Determination," *Global Positioning System: Theory and Applications*, edited by B. Parkinson and J. Spilker, Vol. 64 of *Progress in Astronautics and Aeronautics*, chap. 19, American Institute of Aeronautics and Astronautics, Washington, DC, 1996.

[38] Crassidis, J.L. and Markley, F.L., "New Algorithm for Attitude Determination Using Global Positioning System Signals," *Journal of Guidance, Control, and Dynamics*, Vol. 20, No. 5, Sept.-Oct. 1997, pp. 891–896.